

**Ultrashort pulse two-photon coherent control of a macroscopic phenomena:  
light-induced current from channelrhodopsin-2 in live brain cells**

Cyrille Lavigne<sup>1</sup> and Paul Brumer<sup>1</sup>

*Chemical Physics Theory Group, Department of Chemistry,  
and Center for Quantum Information and Quantum Control, University of Toronto,  
Toronto, Ontario, M5S 3H6, Canada*

(Dated: 9 March 2022)

Coherent control is extended to macroscopic processes under continuous pulsed laser irradiation. Here, this approach is used to analyze the experimentally measured two-photon phase control of currents emanating from a living brain cells expressing channelrhodopsin-2, a light-gated ion channel. In particular, a mechanism is proposed that encompasses more than 15 orders magnitude in time, from the ultrafast dynamics of retinal in channelrhodopsin-2 to the slow dynamics of the neuron current. Implications for other photochemical processes are discussed.

# I. INTRODUCTION

A quantum system interacting with radiation is sensitive to both the intensity of the exciting radiation as well as its phase.<sup>1</sup> The use of the phase content of light to steer quantum behavior, an essential component of the coherent control methodology, has seen numerous successful applications.<sup>2–5</sup> However, past experimental and theoretical investigations have primarily focused on microscopic phenomena, that is on the behavior of molecules after interaction with few pulses of light. Yet the repeated application shaped pulses of light to a macroscopic system can indeed lead to macroscopic phase control, as shown in a recent control experiment performed on brain tissue.<sup>6</sup>

Specifically, Boppart’s group demonstrated that the current emanating from living brain cells expressing channelrhodopsin-2 (ChR2), a light-gated ion channel,<sup>7,8</sup> is sensitive to the phase of a two-photon excitation. In this experiment neurons are exposed to a train of ultrashort chirped pulses over a macroscopically long time (1200 ms). The near-infrared pulses impinging on the neurons photoisomerize retinal in ChR2, thus activating it. Target neurons then evoke an electrical current. Critically, the measured current is found to be sensitive to both the sign and magnitude of the pulse chirp, a pure phase control effect.<sup>9</sup>

In contrast with previous work on the control of biological molecules,<sup>10,11</sup> the demonstrated phase control is macroscopic in both magnitude and time. The measured currents are evoked by the cell over a full second of exposure to light. The dynamics of the electrical response of neurons occur over the millisecond timescale,<sup>7</sup> the excitation and isomerization dynamics of retinal in ChR2 are femto to picosecond processes,<sup>8,12</sup> and the separation between individual laser pulses is on the scale of nanoseconds. Hence, phase control and its effects were found to span a time range of over 15 orders of magnitude.

This experiment provides a demonstration of how weak multiphoton control from ultrafast pulses can lead to macroscopically measurable effects. Similar control could be applied to other isomerization processes<sup>13–15</sup> as well as to photochemical reactions in the condensed phase.<sup>16–18</sup> Quantum control, and in particular phase control, has important potential applications to optogenetics and photochemistry. For example, phase control provides a means of selectively exciting neighbouring molecules that overlap spectrally.<sup>19–24</sup> In scattering media, the exciting field will acquire a spatially dependent phase; phase control is thus also a potential route to superresolution targeting of excitations.<sup>25,26</sup>

The methodology of coherent control provides a rigorous and physically-motivated description of phase coherence and phase interference in light-matter interactions.<sup>1</sup> Physical conditions on interference can be used to devise new control schemes, i.e. methods for phase controllability.<sup>27,28</sup> From a phenomenological point of view, coherent control schemes are also potential mechanisms for experimental phase control obtained in any number of ways, e.g. chirp control<sup>29</sup> or adaptive feedback.<sup>30</sup>

In this article we examine the experiments in Ref. 6 in order to expose the underlying coherent control mechanism. To do so we first develop a theoretical description of two-photon coherent control with ultrashort pulses.<sup>31</sup> Three control schemes are then proposed as feasible mechanisms for the phase-controlled current generation in live brain cells, based on an analysis of possible interference pathways. Spectroscopic means are then described to distinguish and characterize each of the control mechanisms. Importantly, we show that microscopic interference effects due to repeated coherent interactions can accumulate to produce a macroscopic coherent control result, even in the presence of fast decoherence and dissipation. We demonstrate this in a computational study, where a quantum mechanical (minimal) model of retinal<sup>32–34</sup> is coupled to a set of classical rate equations describing the current dynamics of ChR2.<sup>35,36</sup> The multi-timescales model is seen to reproduce the chirp dependence and other qualitative features of the experimental phase control of ChR2.

## II. THEORY

### A. Channelrhodopsin-2

Channelrhodopsins have been extensively studied for their use in optogenetics.<sup>7</sup> An accurate rate model for the millisecond timescale polarization of neuron cells expressing ChR2 has been previously devised,<sup>35–38</sup> and will be helpful in our analyzing the demonstrated phase control of current.<sup>6</sup> Note that the focus here must be on qualitative features of the measured phase-dependent current since a quantitative analysis over all relevant timescales is beyond the state of the art.

The ChR2 protein is thought to exist in four states (see Fig. 1), with distinct spectroscopic and electrochemical properties.<sup>8,35</sup> The protein contains a retinal molecule, which acts as the photoreceptor. The dark-adapted state  $C_1$  is closed to ion transfer into the cell and thus

non-conductive. Light-mediated activation, through retinal photoisomerization, leads to the open conductive state  $O_1$  (with rate  $K_{a1}$ ) which exists in equilibrium with the more stable yet less conductive light-adapted open state  $O_2$ . The forward and backward transitions between  $O_1$  and  $O_2$  are primarily thermally driven, with a weak dependence on the applied light. ChR2 in the  $O_1$  state can relax thermally back to the closed state  $C_1$ , while ChR2 in the  $O_2$  state relaxes to the light-adapted state  $C_2$ . The state  $C_2$  can be activated back to  $O_2$  (with rate  $K_{a2}$ ), also through a photoisomerization. In the absence of radiation however, the protein in the light-adapted state  $C_2$  slowly relax back to the dark-adapted state  $C_1$ . These processes are shown in Fig. 1.

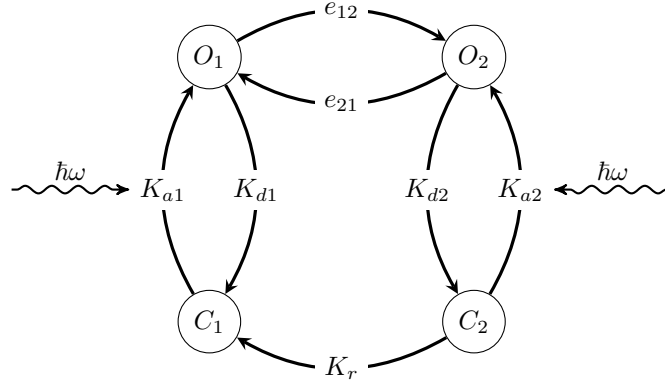


FIG. 1: Four state model of ChR2 from Ref. 35.  $C_1$  and  $O_1$  denotes the non-conductive (i.e., closed) and conductive (open) configurations of the protein in its dark-adapted form, with corresponding light-adapted configurations  $C_2$  and  $O_2$ . Arrows denote transitions between these states with corresponding rates (see Appendix A).

The activation rates  $K_{a1}$  and  $K_{a2}$ , i.e. the rates of the  $C_1 \rightarrow O_1$  and  $C_2 \rightarrow O_2$  transitions, are given by the photoisomerization rate of retinal in ChR2. Importantly, the coherent control of peak current described below results from controlling these activation rates. The rate of photoisomerization is a function of the amount of light received by retinal (i.e. the number of excitations per second) and the quantum yield of isomerization (i.e. the fraction of excitations that goes on to form the final product.) The activation rate for a weak, monochromatic light source with frequency  $\omega$  is given by the standard photochemical expression,

$$K_{ai}(\omega) = \Phi(\omega)\sigma_{\text{ret}}(\omega)\eta_i(\omega) \quad (1)$$

where  $\eta_i(\omega)$  is the quantum yield of isomerization,  $\sigma_{\text{ret}}(\omega)$  is the cross-section of retinal,  $\Phi(\omega)$  is the spectral photon flux, and the cross-section has been taken to be identical for both the dark- and light-adapted states.<sup>37</sup> However, this activation rate formula is not valid in the case of two-photon excitation using a pulsed laser; in particular, the one-photon, monochromatic activation rate is not phase-dependent and thus is not phase controllable. In contrast, the treatment below, that generalizes the activation rate formula to two-photon excitation by trains of ultrashort pulses, is phase-dependent and phase-controllable.

The developments below focus on the coherent control of the peak current resulting from the formation of the dark-adapted open state  $O_1$ . ChR2 current dynamics obtained using the model of Appendix A is demonstrated in Fig. 2 and is obtained via a two-step process. Initially, the current shows a peak which is primarily determined by the rate of formation of  $O_1$  due to excitation from  $C_1$ .<sup>35,39</sup> The peak current is followed by a decay to a steady-state current, with a value determined by the competing rates of formation, decay and interconversion of the dark- and light-adapted open states. At moderate to high laser intensity, control of the peak current<sup>6</sup> is primarily a result of controlling the initial generation of  $O_1$ , which is well-known to be triggered by retinal isomerization within the protein.<sup>39</sup> This latter feature allows us to address the nature of phase control in this system.

## B. Timescales of excitation, control and measurement

Macroscopic coherent control, as observed in Ref. 6, operates on multiple timescales spanning more than fifteen orders of magnitude. Careful study of the dynamical processes at play uncovers, as shown in this section, a hierarchy of separated timescales. Significantly, exploiting these separations is key to understand how control of millisecond dynamics can arise from ultrashort interactions.

Consider the coherent control of a photochemical reaction, e.g. the photoisomerization of retinal, that has a metastable, macroscopically long-lived product with decay rate  $k_p$ . Excitation is performed by a pulsed laser with a field of the following form,

$$\varepsilon(t) = \sum_{n=0}^{n_{\text{pulses}}} \varepsilon_1(t - n\Delta t) \quad (2)$$

where  $n_{\text{pulses}}$  is the total number of pulses in the pulse train with a repetition rate  $k_{\text{rep}} = 1/\Delta t$ , and  $\varepsilon_1(t)$  is the field of a single pulse. The pulses consists of a slow envelope  $A(t)$

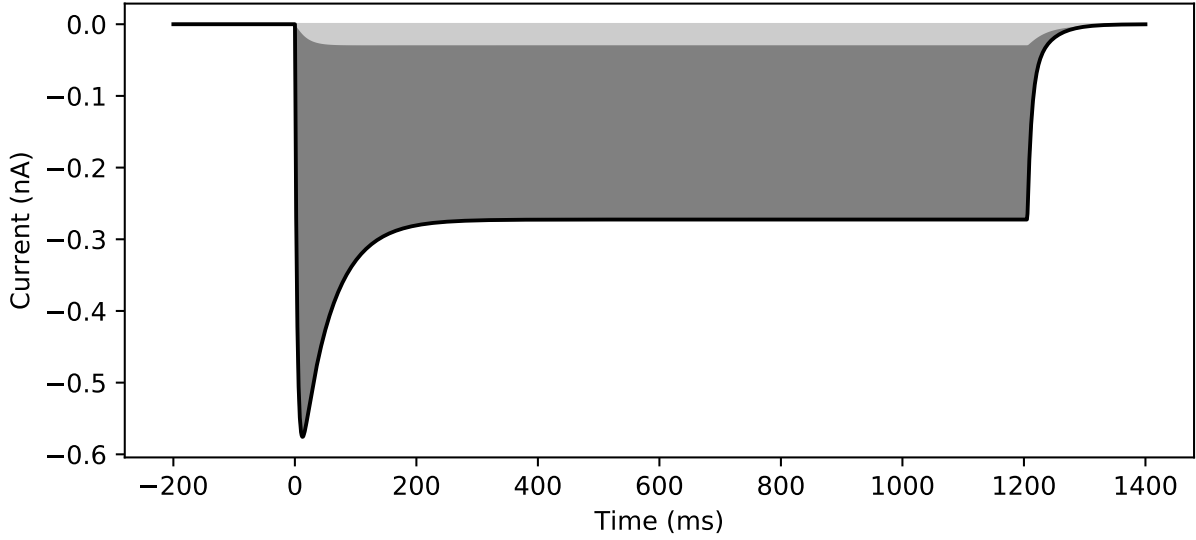


FIG. 2: Current computed from the ChR2 conductance model described in Appendix A for a moderately intense irradiance ( $1 \text{ mW/mm}^2$ ), visible spectrum (470 nm), incoherent light source. The excitation rate of retinal (190 photons per second using the cross-section  $\sigma_{\text{ret}} = 8 \times 10^{-8} \mu\text{m}^{-2}$ ) is comparable to that obtained by two-photon excitation in Ref. 6 and simulations below. Current contributions from the dark- and light-adapted open states of ChR2 are represented by the dark and light grey regions.

with duration  $\sigma_t$  and a carrier frequency  $\omega_c$ ,

$$\varepsilon_1(t) = A(t) \sin(\omega_c t). \quad (3)$$

The single pulse  $\varepsilon_1(t)$  generates coherent dynamics in the molecular system. These dynamics decay with a decoherence time  $\tau_{\text{deco}} = 1/k_{\text{deco}}$ .

Here, two-photon phase control is studied in the case where a strict separation of timescales holds. First, the duration of the pulse  $\sigma_t$  is much slower than the period of the carrier frequency  $\omega_c$ . Pulses are well separated compared to coherent timescales of the system and the field, i.e. the time between pulses ( $1/k_{\text{rep}}$ ) is much longer than  $\sigma_t$  and  $\tau_{\text{deco}}$ . The macroscopic dynamics of the system (with a characteristic time of  $1/k_p$ ) are themselves much slower than the laser pulse train. These temporal relationships can be summarized as follows,

$$1/\omega_c \ll (\sigma_t \text{ and } \tau_{\text{deco}}) \ll 1/k_{\text{rep}} \ll 1/k_p. \quad (4)$$

This is the case, for example, in Ref. 6, where macroscopic control is the result of processes occurring over fifteen orders of magnitude in time: excitation consists of a train of near-infrared ( $1/\omega_c < 1$  fs), ultrashort pulses ( $\sigma_t \approx 0.1 - 1$  ps). The pulses induce ps timescale dynamics, which decay within  $1/k_{\text{deco}} \ll 1$  ns.<sup>40,41</sup> The train has an 80 MHz repetition rate ( $1/k_{\text{rep}} = 16$  ns). Overall control is achieved over the macroscopic current dynamics of a neuron, which are the result of large-scale conformational changes in ChR2, with timescales  $1/k_p \sim 1 - 1000$  ms. Important simplifications can be made based on each of the above relationships to obtain physically motivated coherent control mechanisms for the experiment in Ref. 6. A similar analysis is possible for other experimental scenarios where long-lived photoproducts are obtained from excitation with repeated ultrashort pulses.

### C. Perturbative description of two-photon processes

Two-photon absorption results from the interaction between a quantum mechanical system and a time-dependent electric field at an order quadratic in the intensity of the field. Here, a semiclassical, perturbative description of the light-matter interaction is employed.

Consider a molecule interacting with a time-varying electric field in the dipole approximation.<sup>1,42</sup> The Hamiltonian for such a system is given by,

$$H(t) = H_0 - \varepsilon(t)\mu. \quad (5)$$

where  $H_0$ , the material Hamiltonian, includes everything but the field, i.e., the molecule and its environment,  $\mu$  is the dipole operator and  $\varepsilon(t)$  is the electric field at  $\vec{r}_0$ , the position of the molecule. The corresponding Liouville equation for the density matrix  $\rho(t)$  is

$$\frac{d\rho(t)}{dt} = \mathcal{L}_0\rho(t) + \frac{i}{\hbar}\varepsilon(t)\mathcal{V}\rho(t), \quad (6)$$

with the Liouvillian superoperators  $\mathcal{L}_0\rho = [H_0, \rho]/i\hbar$  and light-matter coupling superoperator  $\mathcal{V}\rho = [\mu, \rho]$ . Provided that the field vanishes sufficiently quickly, the one-photon and

two-photon contributions to  $\rho(t)$  (derived in Appendix B) are given by

$$\rho_2(t) = \left(\frac{i}{2\pi\hbar}\right)^2 \iint_{-\infty}^{\infty} d\omega_2 d\omega_1 e^{i(\omega_2+\omega_1)t+\eta t} \varepsilon(\omega_2) \varepsilon(\omega_1 - i\eta) \quad (7)$$

$$\begin{aligned} & \times \mathcal{G}_0(\omega_2 + \omega_1 - i\eta) \mathcal{V} \mathcal{G}_0(\omega_1 - i\eta) \mathcal{V} \rho_0 \\ \rho_4(t) &= \left(\frac{i}{2\pi\hbar}\right)^4 \iiint_{-\infty}^{\infty} d\omega_4 d\omega_3 d\omega_2 d\omega_1 e^{i(\omega_4+\omega_3+\omega_2+\omega_1)t+\eta t} \varepsilon(\omega_4) \varepsilon(\omega_3) \varepsilon(\omega_2) \varepsilon(\omega_1 - i\eta) \\ & \times \mathcal{G}_0(\omega_4 + \omega_3 + \omega_2 + \omega_1 - i\eta) \mathcal{V} \mathcal{G}_0(\omega_3 + \omega_2 + \omega_1 - i\eta) \\ & \times \mathcal{V} \mathcal{G}_0(\omega_2 + \omega_1 - i\eta) \mathcal{V} \mathcal{G}_0(\omega_1 - i\eta) \mathcal{V} \rho_0 \end{aligned} \quad (8)$$

with the Fourier-domain field and Green's function given by

$$\varepsilon(\omega) = \int_{-\infty}^{\infty} d\omega e^{-i\omega t} \varepsilon(t) \quad (9)$$

$$\mathcal{G}_0(\omega - i\eta) = \frac{1}{i\omega - \mathcal{L}_0 + \eta} \quad (10)$$

The subscripts 2 and 4 in Eq. (7) and Eq. (8) denote the order of the perturbative expansion, which is quadratic in the field amplitude for one-photon processes and quartic in the field amplitude for two-photon processes.

The interaction between the system and radiation yields a frequency dependent measurable change  $I_{\text{diff}}(\omega)$  in the intensity of the laser pulse,

$$I_{\text{diff}}(\omega) = I_{\text{in}}(\omega) - I_{\text{out}}(\omega) \quad (11)$$

where  $I_{\text{in}}(\omega)$  and  $I_{\text{out}}(\omega)$  are the intensity of radiation before and after an interaction with the sample. This value can be computed from the microscopic treatment above provided the sample is highly transparent, as described in Appendix B. In this case, the change in the intensity of the light  $I_{\text{diff}}(\omega)$  as measured by a spectrophotometer is proportional to the spectral number of absorbed photons  $N_{\Delta}(\omega)$  computed for a single interacting molecule. The dimensionless total number of absorbed photons is used below in quantum yield calculation, and is given by

$$N_{\Delta} = \int_{-\infty}^{\infty} d\omega N_{\Delta}(\omega). \quad (12)$$

#### D. Two-photon phase control with an ultrashort pulse

Coherent control of long-lived products arises from interference between multiple indistinguishable light-induced pathways, which is the essence of coherent control.<sup>1</sup> A weaker

form of this statement is useful here, based on frequencies of excitation, as discussed below. The two-photon contribution to the time-dependent expectation value of an operator  $B(t) = \text{Tr} B \rho_4(t)$ , e.g. the isomer population in a photoisomerization process, can be computed from Eq. (8). The integrand has the following oscillatory time-dependence,

$$e^{i(\omega_1+\omega_2+\omega_3+\omega_4)t} \varepsilon(\omega_1) \varepsilon(\omega_2) \varepsilon(\omega_3) \varepsilon(\omega_4) \quad (13)$$

Thus, long-lived control requires that the sum of frequencies  $(\omega_4 + \omega_3 + \omega_2 + \omega_1)$  be close to zero to avoid cancellation via the oscillatory contribution of the exponential.<sup>30</sup> The limited bandwidth of typical ultrashort lasers restricts the number of possible control schemes that satisfies these conditions.

The Fourier transform of the field [Eq. (3)] is given by

$$\varepsilon(\omega) = A(\omega - \omega_c) + A^*(\omega + \omega_c) \quad (14)$$

where the width of  $A(\omega)$  is much narrower than  $\omega_c$ . Thus, both  $\varepsilon(2\omega_c)$  and  $\varepsilon(\omega_c/2)$  are negligible, which reduces the number of possible light-induced interference processes. Indeed, interference is only possible between pathways with the same net number of transitions, e.g., two different two-photon absorption pathways. Other fourth-order processes, such as interference between one-photon and three-photon absorption pathways, lead to fast oscillatory contributions in Eq. (8), with frequencies comparable to  $\omega_c$  or a multiple thereof (i.e. electronic coherent dynamics).

Three control mechanisms can be proposed which account for all possible two-photon interfering pathways respecting the above conditions, and are shown in Fig. 3. Here  $E_i$  and  $E_f$  denote the energy of the initial and final states; the overall energy imparted by the field  $\varepsilon(\omega)$  is  $\Delta E = E_f - E_i$ , which is approximately  $2\hbar\omega_c$  for two-photon absorption, zero for a pump-dump process and  $\hbar\omega_c$  for 1 vs. 3 photon control.

The three control mechanisms of Fig. 3 are best understood in the framework of coherent control.<sup>1,30</sup> Indeed, each control mechanism is also a coherent control scheme — a physically motivated, rationally-designed procedure to control an observable through interference between light-induced pathways.

Consider *2 vs. 2 photon control* (Fig. 3a) where control is the result of interference between a two-photon absorption pathway with frequencies  $\omega_1$  and  $\omega_2$  and a different two-photon absorption pathway with frequencies  $\omega_3$  and  $\omega_4$ . Coherent excitation through both

pathways creates a superposition with the following qualitative form,

$$|\Psi\rangle = \varepsilon(\omega_1)\varepsilon(\omega_2)|\alpha\rangle + \varepsilon(\omega_3)\varepsilon(\omega_4)|\beta\rangle \quad (15)$$

where the two terms in the RHS are the wavefunctions produced by either two-photon absorption pathways. Then, the expectation value of an operator  $B(t)$  resulting from  $|\Psi\rangle$ , e.g. the isomerization probability of an excited molecule, is given by,

$$\begin{aligned} \langle\Psi|B|\Psi\rangle &= |\varepsilon(\omega_1)|^2|\varepsilon(\omega_2)|^2\langle\alpha|B|\alpha\rangle + |\varepsilon(\omega_3)|^2|\varepsilon(\omega_4)|^2\langle\beta|B|\beta\rangle \\ &\quad + 2\text{Re}[\varepsilon(-\omega_1)\varepsilon(-\omega_2)\varepsilon(\omega_3)\varepsilon(\omega_4)\langle\alpha|B|\beta\rangle] \end{aligned} \quad (16)$$

where the Hermitian property  $\varepsilon(-\omega) = \varepsilon^*(\omega)$  has been used. Only the last term, an interference contribution, is sensitive to the phase of the exciting light. Stationary coherent control (i.e. where  $\omega_1 + \omega_2 = \omega_3 + \omega_4$  and where the controlled populations persist after the pulse is over) of this type is shown diagrammatically in Fig. 3a. Similarly, two-photon *pump-dump control* is obtained through interference between different absorption-stimulated emission pathways, with frequencies  $\omega_1, -\omega_2$  and  $\omega_3, -\omega_4$ . A diagram for stationary control of this type, i.e., with  $\omega_1 - \omega_2 = \omega_3 - \omega_4$ , is shown in Fig. 3b. Finally, a one-photon absorption pathway interferes with a pump-pump-dump pathway to obtain *1 vs. 3 photon control* of absorption at  $\omega_c$ , as shown in Fig. 3c. All three control schemes are two-photon (i.e. quadratic in the intensity of light) and coherent (i.e. dependent on the phase of the light).

It should be noted that the diagrams in Fig. 3 are simplifications; Eq. (8) is integrated over all frequencies, and multiple schemes may be operating at the same time. Furthermore, the initial steady state may be a mixture of energy eigenstates, as is the case if, for example, the system is initially thermally distributed. Importantly, the final energy  $E_f$  may be multiply degenerate, allowing for control not only over the transition probability from  $E_i$  to  $E_f$  but also over a particular state at  $E_f$ . This is the case analyzed below, where coherent control modifies both the overall two-photon absorption *and* the final isomer population.

## E. Control amplification from repeated interactions

Two-photon absorption is proportional to the squared peak intensity of the exciting laser.<sup>43</sup> Hence, using a pulsed laser with a high peak intensity, two-photon absorption is

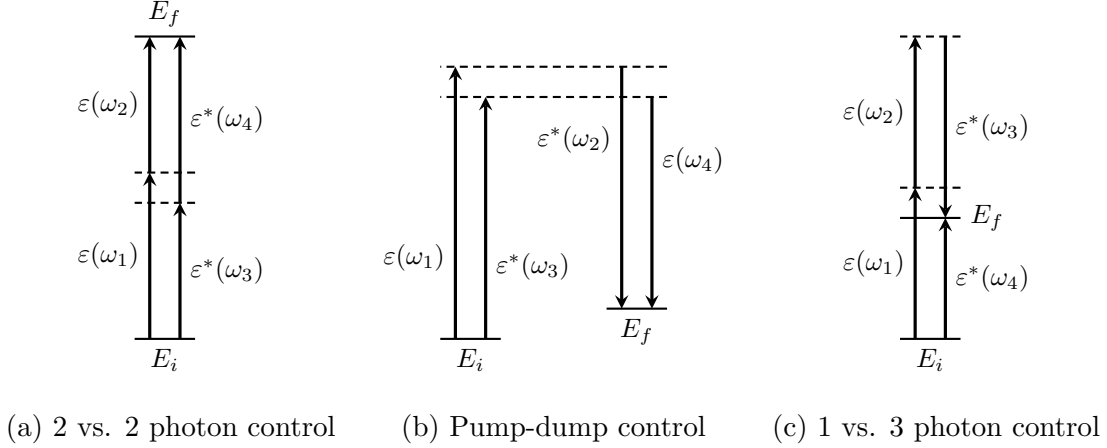


FIG. 3: Three proposed coherent control schemes for stationary phase control in a two-photon pulsed experiment. In each case, the transition probability between initial states with energy  $E_i$  and final states with energy  $E_f$  is a function of the amplitude and phase of the electric field  $\varepsilon(\omega)$  at four distinct frequencies.

possible at a very weak average laser intensity. This well-known property has important consequences for multiphoton control: although each pulse of the laser may excite only a small fraction of the sample, a considerable amount of phase-controllable absorption can be generated due to the interaction with a large number of pulses. This process of control amplification from repeated interactions is described below, with a focus on retinal isomerization in ChR2.

The photoactivation of ChR2 from the non-conductive  $C_1$  state to the conductive  $O_1$  state is driven by retinal photoisomerization. That is, excitation with light triggers the isomerization of primarily all-*trans* retinal in  $C_1$  ChR2 to a mixture of *cis* isomers.<sup>44</sup> The resultant ChR2 in the  $C_1$  protein state containing an isomerized retinal is a precursor to the  $O_1$  state: over a 200  $\mu\text{s}$  interval it forms the open  $O_1$  protein state.<sup>45</sup> If the separation in time between laser pulses  $\Delta t$  is much longer than any coherent dynamics of retinal, and the field is sufficiently weak such that multiple excitations within 200  $\mu\text{s}$  are unlikely, then the rate of formation (in product per second) of  $O_1$  from  $C_1$  can be obtained directly from the product of the repetition rate of the laser (pulses per second) and the probability of an isomerization event occurring from an individual pulse (product per pulse). All these conditions are satisfied in the live brain cell experiments in Ref. 6. The activation rate is

then given by,

$$K_{a1} = k_{\text{rep}} (I_0 P^{(1)} + I_0^2 P^{(2)}) \quad (17)$$

where  $I_0$  is a dimensionless scaling factor for the intensity of the field,  $k_{\text{rep}}$  is the laser repetition rate and  $P^{(1)}$  and  $P^{(2)}$  are the one- and two-photon contributions (from a single laser pulse) to the quasi stationary *cis* population. These are computed perturbatively using Eq. (7) and Eq. (8) as follows,

$$P^{(1)} = \text{Tr}[P_{\text{cis}}\rho_2(T)] \text{ and } P^{(2)} = \text{Tr}[P_{\text{cis}}\rho_4(T)] \quad (18)$$

where  $P_{\text{cis}}$  is the projection operator for the *cis* population,  $\rho_2(T)$  and  $\rho_4(T)$  are the result of excitation from the steady-state ground *trans* state of retinal, and  $T$  is a time much longer than ultrafast coherent dynamics. The  $P^{(2)}$  term is dependent on the laser phase and hence is the origin of the control discussed below.

As noted above, repeated interactions can create a large amount of multiphoton control even from weak pulses. The activation rate from Eq. (17) is seen to depend linearly on the repetition rate of the laser. Thus, the activation rate  $K_{a1}$  can be increased by increasing the repetition rate without affecting the relative contributions from one, two or higher order processes. That is, if the effect produced by a weak pulse is highly phase dependent, the magnitude of control can be made large simply by increasing the repetition rate, up to limits set by the fast (relative to the ms time scale of the induced current) dynamics of ChR2.

A comparison with CW radiation is instructive. A CW field and a pulsed field with the same average power  $W$  will deliver, over a time  $t_{\text{on}}$ , the same average energy  $\langle E \rangle = W t_{\text{on}}$ . However, the resulting excitation dynamics are not the same. The  $N$  photon contribution to the population depends on the  $N$ -th power of overall field intensity before  $t_{\text{on}}$ ,

$$P_{\text{CW}}^{(N)} \propto (t_{\text{on}} I_0)^N. \quad (19)$$

In general, the proportion of each order of the perturbative expansion changes with the intensity of the field *and* the length of irradiation. That is not the case for the pulsed field above, where only the intensity of individual pulses affect the relative proportions of multiphoton processes,

$$P_{\text{pulsed}}^{(N)} \propto k_{\text{rep}} t_{\text{on}} I_0^N. \quad (20)$$

In effect, excitation with two sufficiently separated and sufficiently weak pulses produces twice as much product as excitation with one pulse; absolute yields can thus be increased by increasing the number of interactions through  $t_{\text{on}}$  and  $k_{\text{rep}}$  without a concomitant increase in deleterious higher order transitions that would accompany an increase in the overall intensity of the field or, in the case of continuous irradiation, a longer exposure to light.<sup>43</sup>

### III. RESULTS AND DISCUSSION

Microscopic mechanisms and a physical description of control amplification were proposed above to describe large phase control effects arising from repeated two-photon excitation with ultrafast pulses, of the kind demonstrated in a recent experiment on ChR2-expressing neurons.<sup>6</sup> In the first section below, the physics underlying each of the three proposed coherent control schemes is examined using computationally simple models. In the second section, qualitative experimental features are reproduced using a quantum model of retinal dynamics<sup>32–34</sup> coupled to realistic classical rate equations for ChR2 photocurrents.<sup>35–37</sup>

#### A. Mechanisms of two-photon coherent control

In this section, the three two-photon coherent control mechanisms proposed above are studied using variations of a simple model. Parameters are chosen so as to isolate each of the three control schemes.

A model for each of the three control scheme is constructed by tuning the parameters of the minimal five-level system shown in Fig. 4a. The system has two steady states  $|g\rangle$  and  $|p\rangle$ , the initially populated ground state and the controlled product state. The other three states of the system are unstable *resonances*, due to relaxation processes terminating at either  $|g\rangle$  or  $|e\rangle$ . Relaxation and decoherence are treated in the Lindblad formalism<sup>46</sup> parametrized by rates. By tuning the dipole transition elements  $\mu_{ij}$  and the system energies  $E_i$ , each of the three control schemes can be separately selected, as described below. Parameters that expose each model as well as Lindblad rates are provided in Appendix C.

*Control by a 2 vs. 2 scheme*, shown in blue in Fig. 4b, is obtained through the interference of distinct (i.e. with distinct frequencies  $\omega_1 + \omega_2$  and  $\omega_3 + \omega_4$ ) two-photon pathways in the presence of an intermediate resonance  $|v\rangle$ . The two-photon absorption cross-section to  $|e\rangle$  is

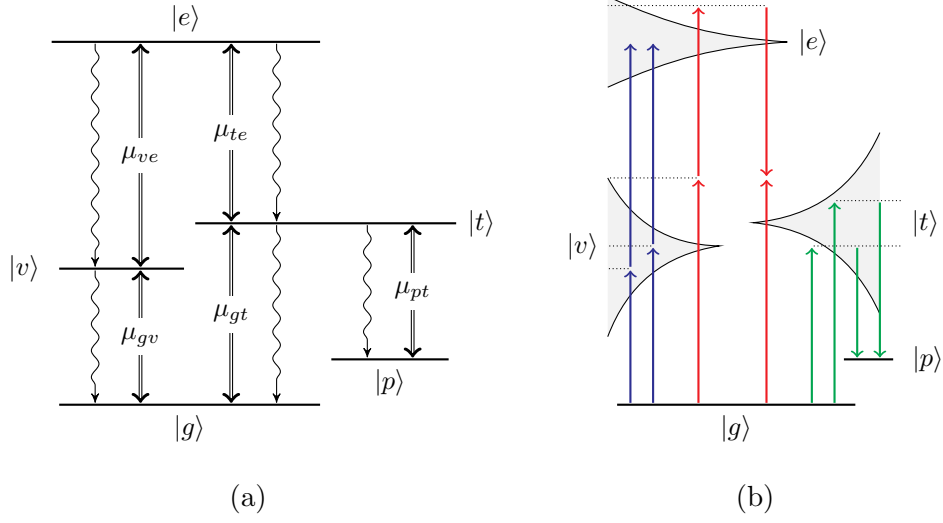


FIG. 4: (a) System used to characterize each of the three control schemes described above.

Solid arrows denote light-induced excitation pathways while curved arrows denote bath-induced relaxation pathways. The states  $|v\rangle$ ,  $|t\rangle$  and  $|e\rangle$  are metastable resonances with finite lineshapes. (b) Excitation pathways for 2 vs. 2 control (blue), 1 vs. 3 control (red) and pump-dump control (green) through the  $|v\rangle$  resonance, the  $|v\rangle$  and  $|e\rangle$  resonances and the  $|t\rangle$  resonance.

then proportional to the product of a one-photon excitation to  $|v\rangle$  followed by a one-photon excitation to  $|e\rangle$ ,

$$T_{g \rightarrow e}^{(2)} \propto I_0^2 |\mu_{g,v} \mu_{v,e}|^2 \quad (21)$$

where  $I_0$  is the intensity of the exciting pulse. If the  $|v\rangle \rightarrow |e\rangle$  transition is significantly brighter than the  $|g\rangle \rightarrow |v\rangle$  transition and the  $|v\rangle$  state is near-resonant, considerable two-photon absorption is obtained without saturating the one-photon  $|g\rangle \rightarrow |v\rangle$  transition. A model for 2 vs. 2 control is obtained here by choosing  $\mu_{ve} = 100\mu_{gv}$  and  $E_v \approx E_e/2$ . Such a model can represent, for example, two-photon near-infrared absorption through a highly excited nearly dark vibrational state.

The *pump-dump control scheme*, shown in green in Fig. 4b, is the result of interference between distinct pump-dump pathways in a manner similar to the 2 vs. 2 control scheme above. Pump-dump control also requires an intermediate resonance (the transition state  $|t\rangle$ ), but excitation to the intermediate resonance is followed by stimulated emission to the final state  $|p\rangle$ , as opposed to further excitation in the 2 vs. 2 control scheme. This control

scheme requires nonzero  $\mu_{g,t}$  and  $\mu_{t,p}$ , which generate a two-photon pathway from  $|g\rangle$  to  $|p\rangle$  via the lineshape of the resonance  $|t\rangle$ . Significant pump-dump control requires  $|p\rangle$  to be of similar energy to  $|g\rangle$ , such that both pump and dump transitions are resonant, another significant difference with the 2 vs. 2 control scheme. Finally, as above, control without saturation is made possible by selecting  $\mu_{t,p} \gg \mu_{g,t}$ , and  $|t\rangle$  to be near resonant with the near-infrared excitation pulse.

Finally, *1 vs. 3 control* arises from interference between a one-photon excitation pathway and a three-photon excitation and stimulated emission pathway. In this model study, the former is provided by a one-photon excitation to the lineshape of  $|t\rangle$  while the latter is the result of a non-resonant two-photon excitation through the resonances  $|v\rangle$  and  $|e\rangle$ , followed by stimulated emission to  $|t\rangle$ . Thus, the 1 vs. 3 contribution obeys the following,

$$T_{g \rightarrow t}^{(2)} \propto I_0^2 |\mu_{g,v} \mu_{v,e} \mu_{e,t} \mu_{g,t}|. \quad (22)$$

The 1 vs. 3 contribution depends linearly on the  $g \rightarrow t$  transition *amplitude*, whereas both the one-photon absorption to  $|t\rangle$  and two-photon absorption to  $|e\rangle$  via the near resonant state  $|t\rangle$  depend quadratically on  $\mu_{g,t}$ . Strong control without saturation and without resonant two-photon excitation thus requires  $\mu_{g,t}$  to be very small compared to  $\mu_{g,v}$ ,  $\mu_{v,e}$  and  $\mu_{e,t}$ . Otherwise, any control will be lost to a high one-photon absorption to  $|t\rangle$  or a high non-resonant two-photon absorption to  $|e\rangle$ . A model for this system is obtained by choosing  $|v\rangle$  to be far from resonance,  $|t\rangle$  to be resonant and  $\mu_{g,t}$  to be small and non-zero.

Of course, it may not be possible to cleanly separate the three control schemes in an experiment. Indeed, depending on the coupling scheme and intensity of the exciting radiation, all three control mechanisms may simultaneously contribute to coherent control. The approach in artificially selecting parameters that promote one or the other control mechanism, as outlined below, is not designed to accurately reproduce control in channelrhodopsin, but rather to expose the similarities and differences between various control mechanisms. In particular, clear experimental signatures of each mechanism by which they can be identified are obtained below, which can be used to rigorously characterize control experimentally.

## 1. Control with chirped excitations

The key experimental result of Ref. 6 shows that control is effected by chirping the exciting pulse. Applying a chirp  $\chi$  to the slow envelope pulse  $\varepsilon(\omega)$  in Eq. (14) above yields,

$$\varepsilon(\omega, \chi) = A(\omega - \omega_0)e^{-i\chi(\omega - \omega_0)^2} + c.c. \quad (23)$$

In the time domain and for a positive chirp, this is equivalent to applying a frequency-dependent delay, wherein the low frequency components of the pulse arrive before the high frequency components. A negative chirp yields the opposite effect. The chirp is a pure phase modification; hence any obtained control is entirely due to phase effects. All three of the above control schemes are sensitive to both the magnitude and sign of the chirp. The exact dependence is a function of the spectral properties at resonance, i.e. the lineshape and frequency of the resonances in Fig. 4.

The effect of chirp on the overall transition probability is shown in Fig. 5 for each of the three control schemes. The computed observable is the amount  $P(\chi)$  of steady-state product formed, up to fourth order in the field amplitude  $\varepsilon(\omega, \chi)$ , given by

$$P(\chi) = \langle p | (\rho_0 + \rho_2(T) + \rho_4(T)) | p \rangle \quad (24)$$

where  $\rho_0 = |g\rangle\langle g|$ ,  $\rho_2(T)$  and  $\rho_4(T)$  are given by Eq. (7) and Eq. (8), and where the field is a near-infrared Gaussian pulse with an unchirped full width at half maximum (FWHM) of 80 fs, a central frequency of 1.38 eV and an applied chirp of  $\chi$ . The time  $T > 10$  ps is well after a new steady state is reached.

All three curves are superficially similar to one another and to that of Ref. 6, showing that the relationship between the excitation probability and the chirp is not sufficient to discern the underlying control mechanism. In all cases, response to the sign of the chirp depends on whether the near-resonant transition is of a lower or higher energy than the exciting pulse, and does not provide additional information about the mechanism. It will be shown below, however, that certain spectral signatures can be used to distinguish each of these control schemes.

The population  $P(\chi)$  depends on the sign of the applied chirp for all three control mechanisms (Fig. 5), as does the experimental control of neuron current. This is due to the presence, in all three models, of a near-resonant one-photon transition. A near-resonant

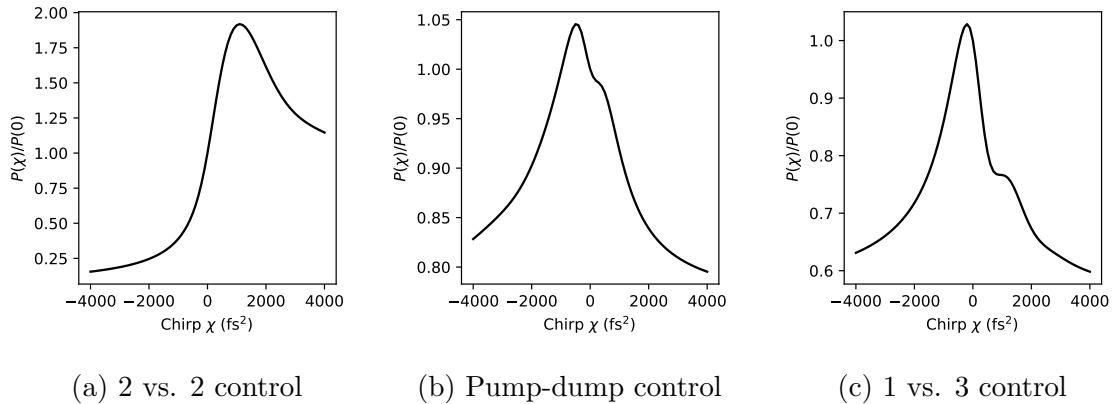


FIG. 5: Probability of forming the product state  $|p\rangle$  normalized by the result at zero chirp for resonant (and hence controllable) models of retinal shown in Fig. 4.

transition is likely to be the source of chirp control in Ref. 6 as well as nonresonant processes are sensitive to the magnitude but not to the sign of the chirp.<sup>47,48</sup>

The magnitude of the chirp determines the delay between high and low frequencies of the pulse; whether low frequencies arrive before or after high frequencies is given by the sign of the chirp. The impact the latter has on control is best described by an example. Consider the case of two-photon absorption through an intermediate state  $|v\rangle$ , represented pictorially in Fig. 6, with two frequencies  $\omega_1$  and  $\omega_2 > \omega_1$ . The two-photon absorption probability is maximized by exciting first to  $|v\rangle$  and then to  $|e\rangle$ . If  $|v\rangle$  is near-resonant with  $\omega_1$  then the transition probability will be maximized when frequency  $\omega_1$  arrives before  $\omega_2$ , i.e. when the chirp is positive (Fig. 6a). However, if  $|v\rangle$  is far from both  $\omega_1$  and  $\omega_2$ , it matters not whether  $\omega_1$  or  $\omega_2$  arrives first; any dependence on the sign of the chirp is lost (Fig. 6b). A similar description can be made for all three control mechanisms.

Hence, in the absence of near-resonant transition, dependence on the sign of the chirp is lost for all three mechanisms. For example, in the 2 vs. 2 case, we can examine this by lowering the system energy of  $|v\rangle$  such that the  $|v\rangle$  lineshape is out of resonance. The same is done with  $|t\rangle$  for the pump-dump. Then, the sign of the chirp no longer affects the transition probability, as shown in Fig. 7. Similarly, in the 1 vs. 3 case, in the absence of a one-photon resonant transition to  $|t\rangle$ , the 1 vs. 3 contribution becomes zero. Then, only the non-resonant two-photon absorption pathway from  $|g\rangle$  to  $|e\rangle$  is bright and all dependence on the sign of the chirp also vanishes.

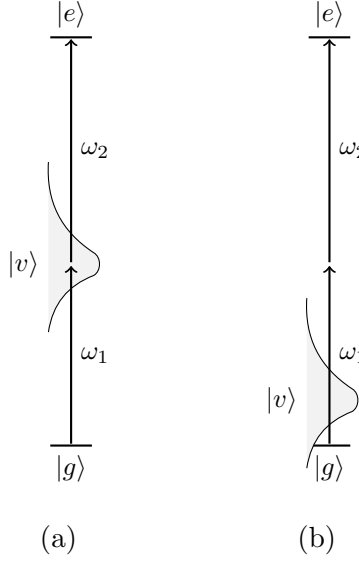


FIG. 6: Pictorial description of two-photon absorption through an intermediate state (a) at or near resonance and (b) far from resonance.  $\omega_1$  and  $\omega_2$  are two frequencies of light, with  $\omega_1 < \omega_2$ .

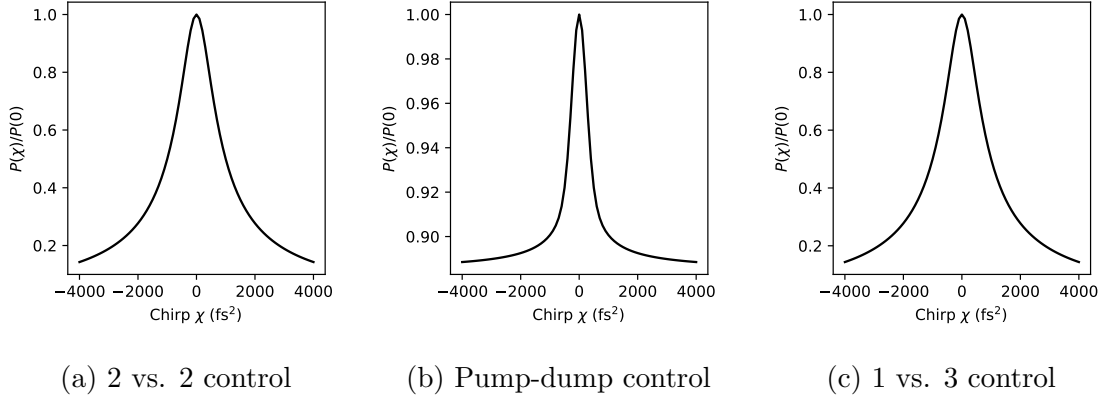


FIG. 7: As in Fig. 5 but without a near-resonant transition. In all cases, light-induced product formation becomes independent of the sign of the chirp, as expected.<sup>21,24,47</sup>

## 2. Absorption and quantum yield

For all three schemes, phase control arises both from a change in overall absorption and from a direct, phase-dependent change in the likelihood of product formation upon absorption, i.e., the quantum yield. The quantum yield of a photoproduct is given by the ratio of formed product to the number of photons absorbed. For the present models, the

quantum  $QY(\chi)$  yield is given by the following function of the chirp  $\chi$ ,

$$QY(\chi) = P(\chi)/N_{\Delta}(\chi) \quad (25)$$

where  $P(\chi)$  is defined in Eq. (24) and the number of absorbed photon is computed from Eq. (12).

Control over the quantum yield is demonstrated in Fig. 8. The quantum yield depends in all three cases on the sign and magnitude of the chirp (i.e., phase controls both the amount and the efficiency of product formation). For the present model, the quantum yields of Fig. 8 are readily explained based on model parameters, specifically the 50% and 80% yields of the  $|e\rangle \rightarrow |t\rangle$  and  $|t\rangle \rightarrow |p\rangle$  transitions. The quantum yield of the two step process from  $|e\rangle$  to  $|p\rangle$  via  $|t\rangle$  is 40%, the product of the yields of the individual steps. Thus, the maximum quantum yield for the 2 vs. 2 control scheme in this model is 20%; two photons are required to form  $|e\rangle$ , which forms the product  $|p\rangle$  40% of the time (The actual value is lower, reflecting the presence of one-photon excitations of  $|v\rangle$  which does not contribute to product formation.) Similarly, the 1 vs. 3 control scenario contains two-photon contributions, with a maximal yield of 20%, as well as direct excitation to  $|t\rangle$ , which has a maximal yield of 80%. The obtained value is significantly lower than the latter. The quantum yield of the pump-dump scheme is somewhat poorly defined,<sup>49</sup> but is similarly phase controllable.

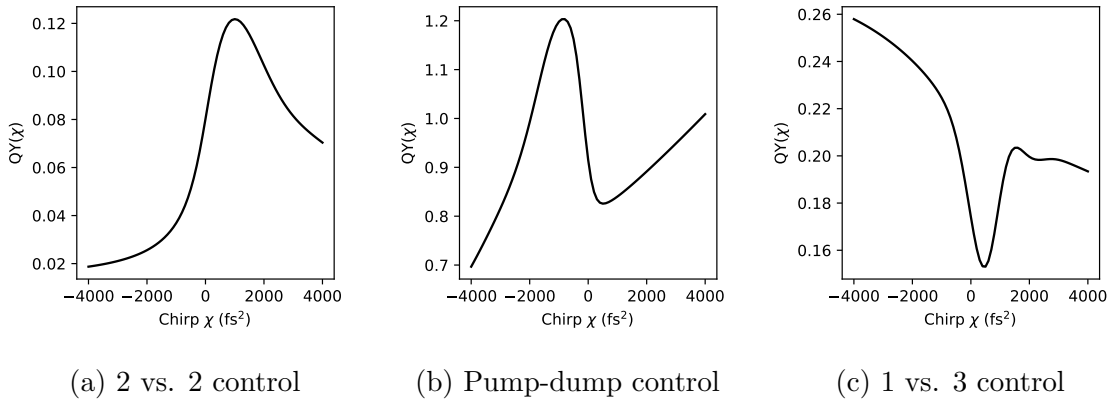


FIG. 8: Quantum yield for the formation of  $|p\rangle$  as a function of chirp computed from Eq. (25).

### 3. *Control mechanisms signatures*

The control obtained as a function of chirp is broadly similar for all three mechanisms (as seen in Fig. 5) and thus provides little or no information about the source of control. However, each of the control schemes results from a specific pattern of interactions with the exciting field, and spectroscopic signatures that can be used to discriminate between the three proposed control schemes are encoded in the outgoing light from the system. Specifically, these interactions produce absorption and stimulated emission peaks, spectroscopic evidence of the control mechanism, in the outgoing radiation. These spectroscopic signatures are discussed below.

Consider then the change in the light intensity, which for a weak pulse is given by Eq. (11). The intensity  $I_{\text{diff}}(\omega)$  contains information both about the field itself and about the system. For linear absorption, the latter can be isolated by computing the transmission,

$$T(\omega) = 1 + I_{\text{diff}}(\omega)/I_{\text{in}}(\omega). \quad (26)$$

However, here the intensity is used instead of the transmission, since the latter is, in the case of multiphoton processes, no longer a property of the material alone but also of the exciting pulse. The two-photon absorption cross-section is similarly affected; the cross-section has a non-trivial dependence on the phase of the exciting light when the excitation is ultrashort and shaped.<sup>21,48</sup> These issues are addressed by directly measuring  $I_{\text{diff}}(\omega)$ , e.g. using a spectrophotometer, but without normalizing by the spectrum of the incoming field. The result is a function of the incoming field but is easily and unambiguously interpreted: it is negative at frequencies where light is absorbed and positive at frequencies where light is emitted.

$I_{\text{diff}}(\omega)$  for the near-resonant 2 vs. 2 case is shown in Fig. 9a. The weak-field case shows absorption by a state at  $\hbar\omega_{v,g} = 1.36$  eV, which is near-resonant with the pulse centered at 1.38 eV. The main visible transition of the system is at  $\hbar\omega_{e,g} = 2.76$  eV. At the intensity corresponding to control shown above, two-photon absorption becomes significant. Absorption from  $|v\rangle$  to  $|e\rangle$  is then seen as a two-photon absorption dip appearing at  $\hbar\omega_{e,v} = 1.40$  eV, with a lineshape reflecting that of the field and of the excited state. Control of this 2 vs. 2 type can thus be identified by the appearance of an absorption peak at higher intensity that is not present in the linear excitation regime.

The equivalent spectra for the pump-dump case is shown Fig. 9b. At low intensity, only absorption at  $\hbar\omega_{g,t} = 1.40$  eV is seen. Increasing the intensity into the control regime leads to appearance of an emissive feature at  $\omega_{t,p} = 1.35$  eV, the dump frequency, where there is no weak-field absorption. Thus, pump-dump control has the opposite signature as 2 vs. 2 control; it can be identified by the appearance of an emission peak at higher intensity that is not present at lower intensity.

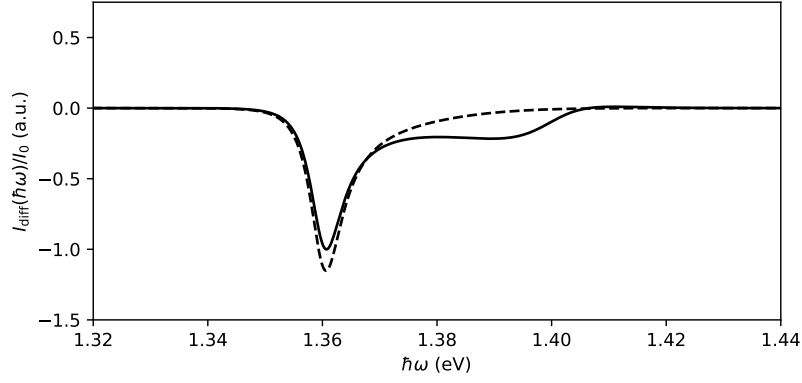
The 1 vs. 3 case, shown in Fig. 9c and 10a, is complicated by the presence of both a non-resonant two-photon pathway and the 1 vs. 3 control pathway. The far-from-resonance  $|v\rangle$  lineshape is responsible for the uniform absorption of the pulse seen in the weak-field spectrum. The very weak  $g \rightarrow t$  transition is responsible for the peak at 1.35 eV.<sup>50</sup> The increase in uniform absorption at higher intensity is the result of non-resonant two-photon absorption through  $|v\rangle$ .

Given these complications, we note an alternate characterization of the 1 vs. 3 control scheme. Specifically, it is characterized by the chirp dependence of the one-photon absorption line. Chirping the pulse, as is shown in Fig. 10a, reveals the control features. In this case, for a positively chirped pulse, the one-photon absorption to  $|t\rangle$  interferes destructively with the pump-pump-dump pathway, even far from saturation. This is the same mechanism that is responsible for the dip in quantum yield in Fig. 8. The same is not seen in 2 vs. 2 control, shown in Fig. 10b. Since the pulse is too low in intensity to saturate the  $|v\rangle$  state a change in the chirp does not significantly affect absorption to  $|v\rangle$ .

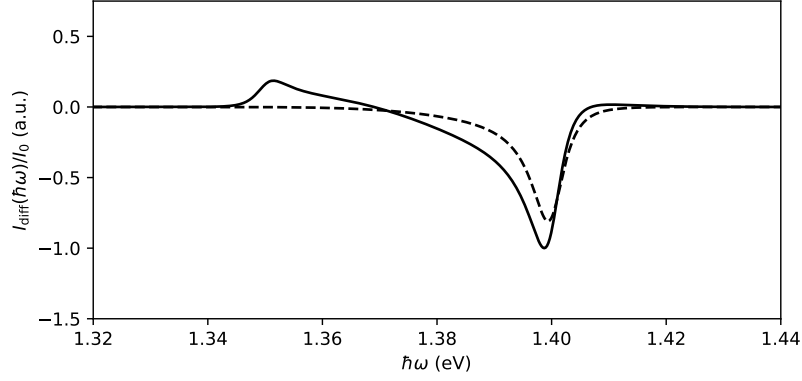
## B. Control of current in ChR2

Control amplification from repeated pulsed laser interactions is demonstrated below and the resultant simulation is shown to reproduce the main qualitative experimental features of control over the peak current of ChR2.<sup>6</sup> Specifically, a model of retinal<sup>34</sup> is used to evaluate the effect of chirp on the photoisomerization of retinal in ChR2. The photoisomerization transition probabilities are then used to compute transition rates for a classical model of a ChR2 expressing neuron.<sup>35–37</sup>

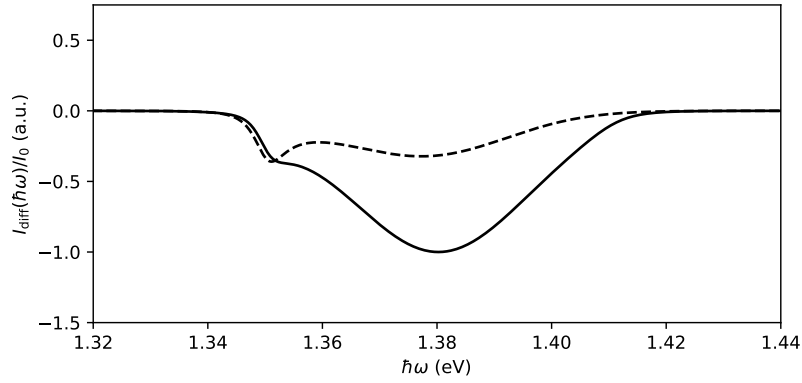
The focus of this section is on the 2 vs. 2 coherent control scheme described above for two reasons: (1) the pump-dump control scenario with a slow-envelope pulse requires the product energy to be similar to the ground energy, and (2) the 1 vs. 3 control scheme



(a) 2 vs. 2 control



(b) Pump-dump control



(c) 1 vs. 3 control

FIG. 9: Change in intensity  $I_{\text{diff}}(\omega) = I_{\text{in}}(\omega) - I_{\text{out}}(\omega)$  for (a) 2 vs. 2, (b) pump-dump, and (c) 1 vs. 3 control for an electric field with an intensity  $I_0 = I_c$  (solid) and a much weaker field with intensity  $I_0 = 10^{-6}I_c$ . Both are normalized by  $I_0$ .  $I_c$  corresponds to the intensity used in Figs. 5-8 at which significant two-photon contributions are present.

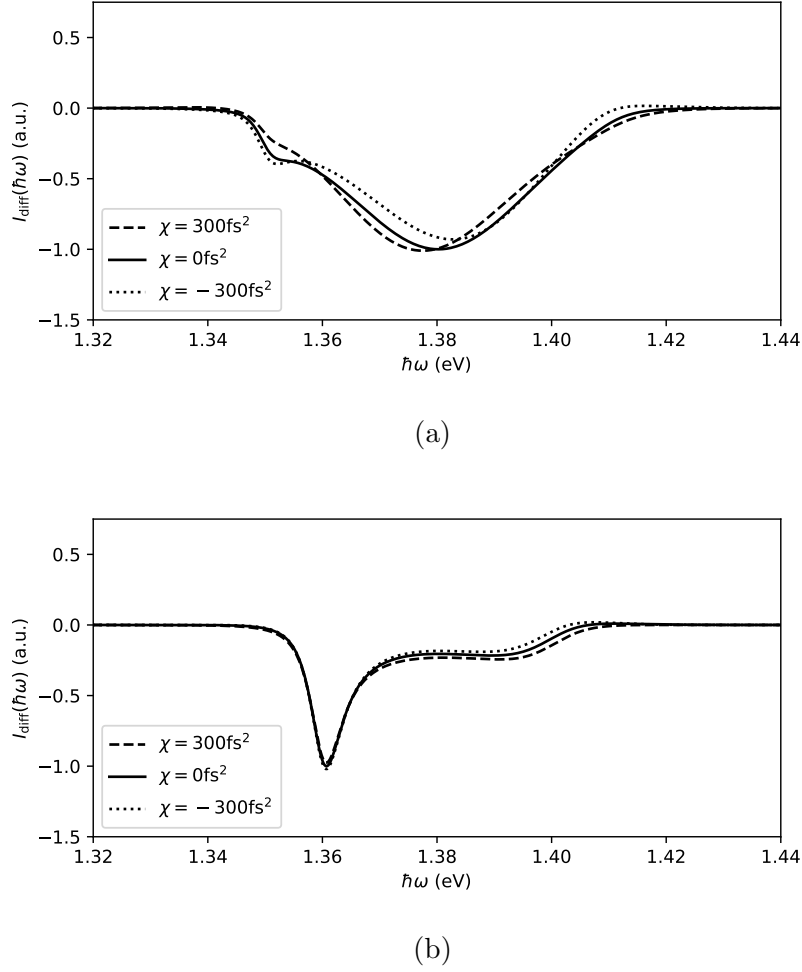


FIG. 10: Change in intensity  $I_{\text{diff}}(\omega)$  for (a) 1 vs. 3 control, and (b) 2 vs. 2 control at three different values of the chirp  $\chi$  and at the control intensity  $I_0 = I_c$ .

requires a delicate balance of the one-photon and three-photon cross-sections. Specifically, with respect to the former and by analogy with other opsins, the isomerization product is likely to have a significantly higher energy than the ground state, since it is this energy storage that drives changes in protein conformation in e.g. bacteriorhodopsin.<sup>51,52</sup> If this is the case also for ChR2, it is unlikely that a direct pump-dump route exists (or is sufficiently bright) to support a pump-dump control scheme. Specifically, with respect to the latter, the 1 vs. 3 control scheme, although possible, is not easily implemented in the more complex model used here without significant fine-tuning. Hence, an analysis of the 1 vs. 3 control scheme awaits further experimental results. By contrast, 2 vs. 2 control is robust, requiring only the presence of a bright near-resonant transitions. The presence of such transitions is

further supported by the high two-photon absorption cross-section of opsins.<sup>39,53,54</sup>

### 1. *Chirp control of retinal isomerization*

Control over the peak current, the quantity of interest here, is the direct result of coherent control over the photoisomerization of retinal in ChR2. At the moderate intensities of interest, the peak current is directly proportional to the population of ChR2 in the dark-adapted, highly conductive open state  $O_1$ , shown in Fig. 2. A transition from the initial  $C_1$  state to the open  $O_1$  state follows the isomerization of a retinal molecule in ChR2;<sup>7,40,41,45,55</sup> thus, the rate of retinal photoisomerization directly determines the peak current. Chirp control over photoisomerization is demonstrated in this section.

The model of retinal described in Appendix D has two quasi-steady states, corresponding to *cis* and *trans* isomers of retinal, with the ground state being of fully *trans* character. The result of a one-photon excitation at 2.5 eV is demonstrated in Fig. 11a. Transient dynamics is seen to be followed by a ps relaxation to a stable distribution of isomer populations. The transient dynamics during and just after the pulse, but not the steady state population, are seen to be phase dependent. The particular form of the bath establishes a high quantum yield of  $\approx 0.75$  (not shown) for the isomerization, consistent with experiment.

Two-photon chirp control is obtained by modifying this model to include a near-resonant one-photon transition at half the one-photon excitation energy. That is, we added a bright *trans* state  $|v\rangle$  at 1.22 eV from the ground state (i.e. in the near infrared), thus creating control of the 2 vs. 2 type.<sup>56</sup> For simplicity, the state  $|v\rangle$  is taken to be vibrationally identical to  $|g\rangle$ . Furthermore,  $|v\rangle$  relaxes to  $|g\rangle$  in 200 fs; as such, it does not lead to any isomerization. Such a state may represent, for example, a highly excited vibrational state from an anharmonic mode of retinal. The transition dipole operator is taken to be of the form,

$$\mu = a_v \mu_v + a_e \mu_e \quad (27)$$

where  $\mu_v = |g\rangle \langle v| + \text{h.c.}$  consists of only the transition between  $|g\rangle$  and  $|v\rangle$  and  $\mu_e$  includes all other transitions.

The parameter  $a_v$  changes the amplitude of one-photon excitation to  $|v\rangle$  while the parameter  $a_e$  sets the transition amplitude of one-photon excitation to  $|e\rangle$  from  $|g\rangle$  and from

$|v\rangle$ . Hence, changing those parameters modifies the cross-sections for one- and two-photon absorption and thus the one- and two-photon isomerization probabilities  $P^{(1)}$  and  $P^{(2)}$  in Eq. (17). The two isomerization contributions from Eq. (18) obey the following simple relations with respect to  $a_v$  and  $a_e$ ,<sup>57</sup>

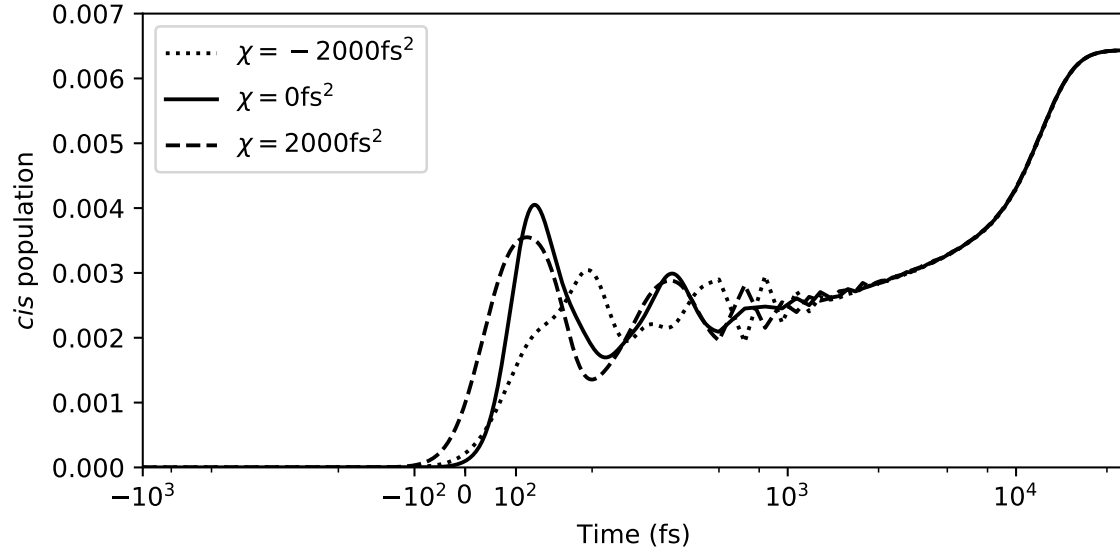
$$P^{(1)} \propto |a_e|^2 \text{ and } P^{(2)} \propto |a_v|^2 |a_e|^2. \quad (28)$$

Hence, experimental measurements of one- and two-photon absorption cross-section fully constrain the values of  $|a_v|^2$  and  $|a_e|^2$ , provided that these measurements are performed at the same near-infrared frequency. In the absence of such direct measurements, the near-infrared one-photon cross-section is estimated from experimental data in Ref. 39 (where a similar laser to Ref. 6 was used) as follows. The peak intensity at which two-photon and one-photon excitation rates are the same is approximately  $I_{\text{same}} \approx 1.7 \times 10^{24}$  photons  $\text{cm}^{-2}$   $\text{s}^{-1}$ . The two-photon cross-section is reported as  $\sigma_2 = 10^{-50}$   $\text{cm}^4$  s photons $^{-1}$ . Hence, the one-photon cross-section  $\sigma_1$  in the near infrared can be computed from

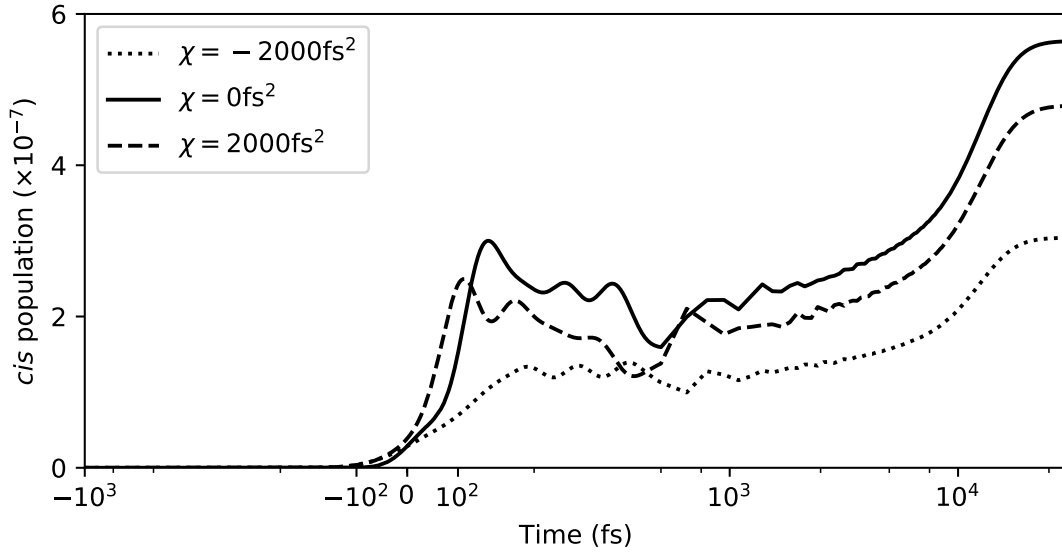
$$P^{(1)} = I_{\text{same}} \eta_1 \sigma_1 = P^{(2)} = I_{\text{same}}^2 \eta_2 \sigma_2 / 2. \quad (29)$$

where  $\eta_1$  and  $\eta_2$  are the quantum yield of near-infrared one-photon and two-photon excitations and  $\sigma_1$  is the near-infrared one-photon cross-section. As an approximation, the two efficiencies are taken to be the same ( $\eta_1 = \eta_2$ ), thus fully determining the values of  $|a_e|^2$  and  $|a_v|^2$ . We note that at the peak intensity of the control laser of Ref. 6 ( $I_c = 5.08 \times 10^{24}$  photons  $\text{cm}^{-2}$   $\text{s}^{-1}$ ) one-photon contributions are still significant; that is, contributions from the one-photon cross-section in the near infrared can not be ignored.

Two-photon excitation, as shown in Fig. 11b, follows similar dynamics to the one-photon excitation of Fig. 11a. This is unsurprising as the  $|v\rangle$  state was taken to be vibrationally identical to the ground state. However, significantly, chirping the pulse now affects *both* the transient dynamics and the steady state isomer populations. Since the state  $|v\rangle$  is near resonant, the isomerization is highly phase controllable (Fig. 12), even though less than one molecule out of a million actually undergoes isomerization. The computed dependence of the photoisomerization probability on the chirp of the exciting pulse shown in Fig. 12 is similar with respect to the chirp sign and amplitude to that reported experimentally.<sup>6</sup>



(a) One-photon excitation



(b) Two-photon excitation

FIG. 11: Population of the *cis* isomer shortly after excitation. In the (a) one-photon case, the pulse central frequency is given by  $\hbar\omega = 2.5$  eV, while it is exactly half that in the (b) two-photon case. The FWHM of the unchirped pulse is 120 fs in both cases. Note the difference in ordinate scale in panels (a) and (b).

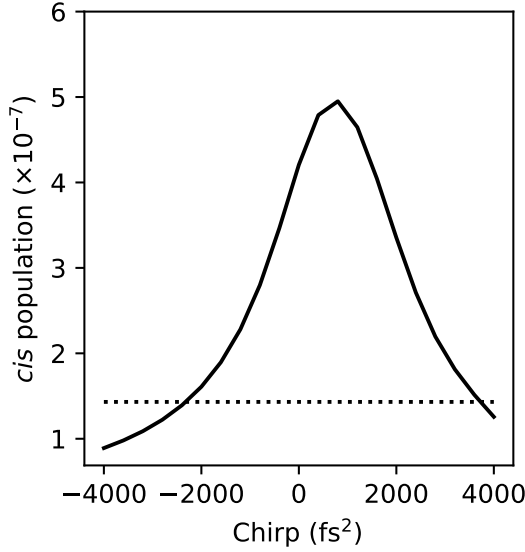


FIG. 12: (a) Two-photon (solid) and one-photon (dotted) contributions  $P^{(2)}$  and  $P^{(1)}$  to the *cis* population after excitation. The (unchirped) excitation pulse has a FWHM of 120 fs and a central frequency of  $\hbar\omega = 1.25$  eV.

## 2. Macroscopic phase control through repeated interactions

The single pulse photoisomerization probability obtained above can be used to compute the  $C_1 \rightarrow O_1$  activation rate  $K_{a1}$  under illumination with a train of such pulses, as given by Eq. (17). The peak current, at laser powers of interest, is principally a function of this activation rate, as shown in Fig. 2. Thus, the phase control demonstrated above should be reflected in an equivalent control of the peak current. The activation rate  $K_{a1}$  was computed using Eq. (17) from the isomerization probability due to a single pulse (Fig. 12) and is shown in Fig. 13a. The obtained peak current (here normalized by the value at zero chirp) is seen to depend both on the magnitude and sign of the applied chirp. *The experimental dependence on the chirp obtained in Figs. 2a and 2c of Ref. 6 is seen to be well reproduced.*

The non-controllable one-photon excitation (dotted line in Fig. 12) lowers the magnitude of phase control such that the peak current (Fig. 13a) has a weaker dependence on the chirp than does the two-photon photoisomerization probability (Fig. 12). Specifically, at high magnitude of the chirp, the two-photon contribution decays to zero; the peak current is then entirely the result of chirp-independent one-photon photoisomerization. This was

noted by Paul *et al.* but was attributed to saturation of the light absorption, which is not the case here, as is demonstrated in the current traces of Fig. 13b. That is, the peak current at saturation is a parameter of the model, here taken to be  $I_{\text{max}} = 2.05 \text{ nA}$ , far larger than the current that is generated here. Neither is the retinal transition saturated, as only a small amount of retinal is excited by each pulse (Fig. 11b). Rather, what limits the amount of control is the presence of one-photon excitations (dotted line in Fig. 12), which are not phase-dependent. Significantly, the ratio of one-photon and two-photon absorption can be modified by changing the repetition rate and intensity of the laser, hence verifiable experimentally.

The amplification of control from repeated interactions is responsible for the chirp-independent linear relationship between the repetition rate and the peak current (Fig. 14a). Indeed, increasing the number of pulses per second produces a corresponding linear increase in the rate of photoproduct formation, as described by eq. (17). Furthermore, the linear relationship is phase-independent; a high relative phase control (a significant change in the photoproduct generated per pulse due to phase control) can be converted to a high absolute amount of phase control (a significant change in the actual quantity of photoproduct generated in the experiment) by increasing the repetition rate.

Changing the repetition rate in this way corresponds to changing the average laser power while keeping the peak power, and thus the relative amount of one-photon and multiphoton absorption processes, fixed. This is in contrast with the result obtained from changing the overall laser intensity, as obtained from e.g. applying a neutral density filter. Then, the proportion of two-photon and one-photon absorption processes, and therefore the amount of phase control, changes nonlinearly, as shown in Fig. 14b. Reducing the intensity leads to a reduction of phase control due to the rapid loss of two-photon absorption and the lack of phase-sensitivity of the one-photon terms (Fig. 11a). This effect is in agreement with the experiment of Ref. 6. Specifically, the peak current was found to be a function  $I^\alpha$  of the laser intensity  $I$ , with  $\alpha$  less than the two-photon expected value of two (Ref. 6, Supplemental Fig. 6). A reduction in intensity was also shown to dampen the effect of the chirp on the peak current. Significantly, both results are readily explained by the amplification mechanism and the presence of a significant, phase-independent one-photon contribution. In addition, this mechanism is valid in the regime where neither the absorption of retinal nor the dynamics of ChR2 are close to saturation, which is consistent with the scaling study of Ref. 39, and

reproduces, as described above, the nonzero peak current detected at high magnitude of the chirp.

Thus, repeated weak interactions were shown here to generate large phase controllable currents. Significantly, control amplification can be experimentally distinguished from other processes by measuring the magnitude of phase dependence at different repetition rates and laser intensities. Furthermore, by increasing the laser intensity while simultaneously decreasing the laser repetition rate, control can be made stronger without saturating either the initial absorption process or the generation of current. The same protocol can be applied to other multiphoton photochemical processes induced ultrafast pulsed lasers.

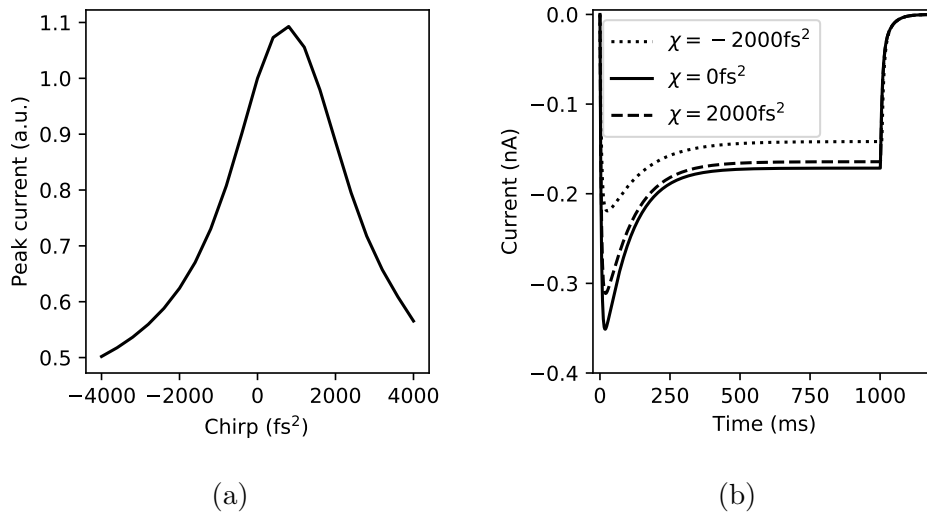


FIG. 13: (a) Peak current as a function of chirp and (b) obtained current traces at three different chirp values for the ChR2 model. Qualitative agreement is obtained with Figs. 2a and 2c of Ref. 6.

#### IV. CONCLUSION

A theory for two-photon phase control of a macroscopic phenomena, such as the experimental control by light of electrical current in live neurons, has been described. Three microscopic mechanisms based on the properties of the exciting field have been proposed with measurable spectroscopic signatures. Under certain assumptions, microscopic control provided by individual pulses in a pulse train accumulates, leading to a large phase effect,

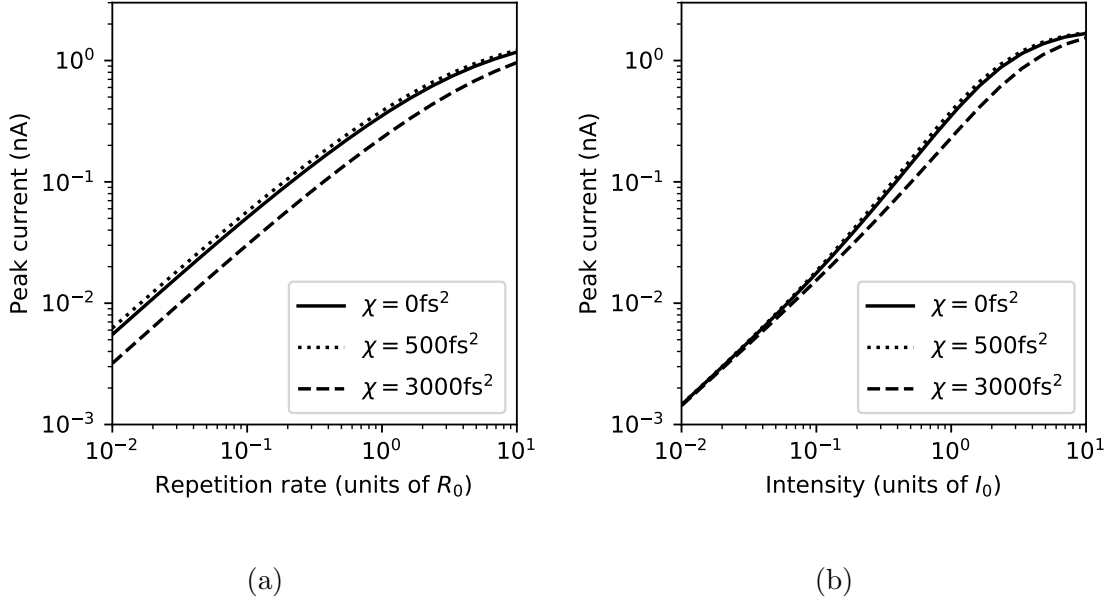


FIG. 14: Peak current for different values of (a) the repetition rate and (b) the peak intensity of the excitation laser, keeping all other parameters fixed, at different values of the applied chirp.  $R_0$  and  $I_0$  denote the repetition rate (80 MHz) and laser peak intensity ( $5.08 \times 10^{24} \text{ photons cm}^{-2} \text{ s}^{-1}$ ) used in Figs. 12 and 13. Note the logarithmic scale of both the ordinate and the abscissa.

which may persist over macroscopic timescales.

A model for the experiment of Paul *et al.* on the coherent control of electrical currents emanated from living brain tissue expressing ChR2, was proposed.<sup>6</sup> Specifically, a quantum mechanical model of retinal<sup>32–34</sup> with experimentally derived one- and two-photon absorption cross-sections<sup>39</sup> was used to compute quantum mechanical isomerization probabilities. These were applied to derive activation rates for ChR2 under repeated pulsed excitation. The ms current dynamics of ChR2-expressing neurons were computed using a set of rate equations.<sup>35–37</sup> This multi-timescale model was shown to reproduce the dependence of the peak current on the chirp of a pulsed laser excitation observed experimentally. The microscopic mechanism of control is consistent with interference between two-photon excitation routes (i.e. 2 vs. 2 photon control) arising from a near resonant transition.

The microscopic mechanism and subsequent control amplification processes proposed here are experimentally verifiable. The control scheme requires the presence of measurable bright near-resonant transitions and has a specific spectral signature (Fig. 9a). Control

amplification through repeated interactions is testable by changing excitation parameters, namely the repetition rate and the intensity of the laser; the effect of chirp on the peak current depends only on the latter (Fig. 14). That is, the ratio of peak current obtained at different  $\chi$  is relatively constant as a function of the repetition rate which is not the case for changes in laser intensity.

Other features of the two-photon excitation of ChR2<sup>6,39</sup> are readily accounted for by the present model: the peak current is a function of the intensity  $I^\alpha$ , with  $\alpha$  between one (linear) and two (quadratic), the effect of the chirp on the peak current is dampened when the intensity is reduced, and the peak current does not fully vanish at high values of the chirp. These features also appear in this model study and are explained as the result of nonzero phase-independent one-photon excitations.<sup>28,58–60</sup> The one-photon contribution can be directly measured by increasing the laser intensity while reducing the repetition rate, i.e. by reducing the laser peak power while keeping fixed the laser average power.

Future work should include more realistic treatment of retinal in ChR2 and of neuron current dynamics. The simulation presented here is primarily a qualitative proof of concept for the described control mechanisms. A quantitative treatment necessitates a more advanced model of retinal in ChR2, informed, e.g., by near-infrared spectroscopy data.<sup>41</sup> In particular, two-photon absorption was included here somewhat artificially; more complete data on one-photon and two-photon near-infrared absorption in ChR2, including which vibrational modes and which electronic states are active, would greatly improve modeling. The role of the retinal environment is of particular theoretical interest. Significantly, the Redfield treatment used here imposes too broad Lorentzian linewidths, thus exaggerating absorption far from resonances. Large system closed dynamics<sup>9,61–63</sup> and non-Markovian methods<sup>64–68</sup> can be used to obtain more realistic, e.g. Gaussian, lineshapes. Finally, a treatment of the neuron biophysics which includes activation dynamics<sup>37</sup> is required to obtain the other phase effect reported in Ref. 6, i.e., that the chirp of the exciting laser changes the spiking pattern of neurons.

The use of more complex pulse shapes to selectively activate specific opsins is particularly interesting for optogenetics applications. For example, different neurons can be made to express different opsins, but selective excitation of opsins is currently limited by a high degree of spectral overlap between different species.<sup>8</sup> Phase control provides an entirely new dimension beyond simple spectral control, which could generate significantly better discrim-

ination between types of opsins, as was previously demonstrated for two-photon induced fluorescence.<sup>19–24</sup> Another avenue for selective excitation is through spatiotemporal control, where both the spatial and temporal phase of light are modulated.<sup>25,26</sup> Joint spatiotemporal focusing and two-photon phase control may be of use in high resolution targeting of individual neurons and dendrites.<sup>69</sup>

The present analysis can also be applied to other photochemical processes where fast two-photon excitation generate macroscopically long-lived photoproducts, e.g. the photoisomerization of azobenzenes,<sup>13–15</sup> the excitation of phosphorescent molecules<sup>70</sup> and the photodissociation of molecular species.<sup>16–18</sup> The repeated application of weak pulses can rapidly create a large phase-controllable amount of photoproducts in the manner described here, provided certain conditions are met. Denoting the time between pulses by  $\tau$ , a similar treatment to this one is possible when (1) the microscopic timescales of coherence and product formation are much shorter than  $\tau$ , (2) the macroscopic timescales of interest are much longer than  $\tau$ , and (3) only a fraction of the system is excited by each individual pulse. For a MHz laser repetition rate, complete formation of products and decoherence must occur within 1  $\mu$ s of excitation, while other macroscopic processes, e.g. decay or removal of photoproducts, must have characteristic timescales much longer than a  $\mu$ s. This type of separation of timescales is common in photochemical and photobiological processes.

**Acknowledgments:** This work was supported by the U.S. Air Force Office of Scientific Research under Contract No. FA9550-17-1-0310, and by the Natural Sciences and Engineering Research Council of Canada.

## Appendix A: Current dynamics of ChR2-expressing neurons

The macroscopic current produced by neurons expressing channelrhodopsin-2 is evaluated using a classical rate model, with empirically determined rates taken from Ref. 35 and Ref. 36. The four-state conductance model (Fig. 1) is simulated using the following rate

equations,

$$\frac{dC_1(t)}{dt} = -K_{a1}C_1(t) + K_rC_2(t) + K_{d1}O_1(t) \quad (\text{A1})$$

$$\frac{dC_2(t)}{dt} = -(K_{a2} + K_r)C_2(t) + K_{d2}O_2(t) \quad (\text{A2})$$

$$\frac{dO_1(t)}{dt} = K_{a1}C_1(t) - (K_{d1} + e_{12})O_1(t) + e_{21}O_2(t) \quad (\text{A3})$$

$$\frac{dO_2(t)}{dt} = K_{a2}C_2(t) - (K_{d2} + e_{21})O_2(t) + e_{12}O_1(t). \quad (\text{A4})$$

The rates for each process are given in Table I. The neuronal current is obtained from

$$I(t) = I_{\max}(O_1(t) + sO_2(t)), \quad (\text{A5})$$

where  $s$  is the ratio of the conductivity of the light- and dark-adapted open states.

The activation rates  $K_{ai}$  of the model for an incoherent blue light source were obtained by a fit to the empirical Hill equation,<sup>36</sup>

$$K_{ai} = k_i \frac{\Phi^p}{\Phi^p + \Phi_m^p} \quad (\text{A6})$$

where  $i = 1, 2$ ,  $\Phi$  is the photon flux in  $\text{m}^{-2} \text{s}^{-1}$ ,  $p$  is a parameter near unity and  $k_i$  has units of time. This nonlinear equation is used to reproduce nonlinear saturation effects at high intensity. This nonlinear form is not based on the physics of light-matter interactions. As this treatment focuses on the weak field regime away from saturation, the following physically-motivated linear form is used instead,

$$K_{a1} = \eta_1 \sigma_{\text{vis}} \Phi \text{ and } K_{a2} = \eta_2 \sigma_{\text{vis}} \Phi. \quad (\text{A7})$$

where  $\eta_1$  and  $\eta_2$  are the quantum yields of dark- and light-adapted ChR2,  $\Phi$  is the photon flux and  $\sigma$  is the cross-section of retinal, assumed here to be the same for both states. At the intensity of interest, Eq. (A6) is nearly linear for both dark- and light-adapted states; a linear fit of this equation provides the quantum yields  $\eta_1$  and  $\eta_2$  given in Table I and the visible-light cross-section  $\sigma_{\text{vis}} = 8 \times 10^{-8} \mu\text{m}^{-2}$ . For two-photon absorption, the dark-adapted activation rate  $K_{a1}$  is computed from the retinal model using Eq. (17). The light-adapted activation rate, which has a negligible impact on the peak current, is estimated here from the zero chirp dark-adapted activation rate  $K_{a1}^{(0)}$ ,

$$K_{a2} = \frac{\eta_2}{\eta_1} K_{a1}^{(0)}. \quad (\text{A8})$$

	$K_{d1}$	$K_{d2}$	$e_{12}$	$e_{21}$	$K_r$
light off <sup>†</sup>	130 s <sup>-1</sup>	25 s <sup>-1</sup>	22 s <sup>-1</sup>	11 s <sup>-1</sup>	0.4 s <sup>-1</sup>
light on*	”	”	53 s <sup>-1</sup>	23 s <sup>-1</sup>	”
	$\eta_1$	$\eta_2$	s	$I_{\max}$	
Both <sup>†</sup>	0.50	0.10	0.05	-1.85 nA	

<sup>†</sup>: Ref. 35, inset of Fig. 8.

\*: *ibid.*, p. 408.

TABLE I: Parameters of the macroscopic model of ChR2 used to compute currents produced by neurons after two-photon excitation. All parameters were taken from Ref. 35.

## Appendix B: Perturbative description of weak-field two-photon absorption and numerical evaluation

In this section, a derivation for Eq. (7) and (8) is provided. The starting point of this analysis is the Liouville equation given by Eq. (6). The following time-dependent Green's function is defined,

$$\mathcal{G}_0(t - t_0) = \Theta(t - t_0) e^{\mathcal{L}_0(t - t_0)}, \quad (\text{B1})$$

where  $\Theta(t)$  is the Heaviside step function. A perturbative expansion to fourth order in the field is necessary to expose all processes quadratic in the field intensity. The terms of the perturbative series are given by

$$\rho_0(t) = \mathcal{G}_0(t - t_0) \rho(t_0) \quad (\text{B2})$$

$$\rho_1(t) = \left(\frac{i}{\hbar}\right)^1 \int_{t_0}^{\infty} dt_1 \varepsilon(t_1) \mathcal{G}_0(t - t_1) \mathcal{V} \rho_0(t_1) \quad (\text{B3})$$

$$\rho_2(t) = \left(\frac{i}{\hbar}\right)^2 \iint_{t_0}^{\infty} dt_2 dt_1 \varepsilon(t_2) \varepsilon(t_1) \mathcal{G}_0(t - t_2) \mathcal{V} \mathcal{G}_0(t_2 - t_1) \mathcal{V} \rho_0(t_1)$$

...

Here, the state at  $t_0$  before the field is on is taken to be a steady state, such that  $\mathcal{G}_0(t - t_0) \rho(t_0) = \rho_0$ . The lower bound  $t_0$  of the integrals is extended to  $-\infty$ . The field is expanded

into its Fourier components to obtain,

$$\begin{aligned}\rho_1(t) &= \left(\frac{i}{\hbar}\right)^1 \int_{-\infty}^{\infty} d\omega_1 \varepsilon(\omega_1) \int_{-\infty}^{\infty} dt_1 e^{i\omega_1 t_1} \mathcal{G}_0(t - t_1) \mathcal{V} \rho_0 \\ \rho_2(t) &= \left(\frac{i}{\hbar}\right)^2 \iint_{-\infty}^{\infty} d\omega_2 d\omega_1 \varepsilon(\omega_2) \varepsilon(\omega_1) \iint_{-\infty}^{\infty} dt_2 dt_1 e^{i\omega_2 t_2 + i\omega_1 t_1} \mathcal{G}_0(t - t_2) \mathcal{V} \mathcal{G}_0(t_2 - t_1) \mathcal{V} \rho_0 \\ &\dots\end{aligned}\tag{B4}$$

The Fourier integrals thus exposed can be used to transform the Green's functions. Certain properties of the field, applicable to ultrashort pulses, are necessary for this transform to be well-behaved.

Consider the following integral,

$$F(t_2) = \int_{-\infty}^{\infty} d\omega_1 \varepsilon(\omega_1) \int_{-\infty}^{\infty} dt_1 e^{i\omega_1 t_1} \mathcal{G}_0(t_2 - t_1) \tag{B5}$$

$$= e^{i\omega_1 t_2} \int_{-\infty}^{\infty} d\omega_1 \varepsilon(\omega_1) \int_0^{\infty} d\tau e^{-(i\omega_1 - \mathcal{L}_0)\tau} \tag{B6}$$

where  $\tau = t_2 - t_1$ . The second integral converges provided that the spectrum of  $(i\omega_1 - \mathcal{L}_0)$  is entirely positive. If that is the case, the following is obtained,

$$F(t_2) = e^{i\omega_1 t_2} \int_{-\infty}^{\infty} d\omega_1 \varepsilon(\omega_1) \frac{1}{i\omega_1 - \mathcal{L}_0} \tag{B7}$$

The eigenspectrum of  $\mathcal{L}_0$  is entirely imaginary for a closed system, with eigenvalues  $i\omega_{nm}$  for every coherence obtained from a pair of eigenenergies  $n, m$  and zero eigenvalues for every population of an eigenenergy. Redfield or Lindblad equations contain decaying contribution (due to decoherence and dissipation); the corresponding Liouvillian thus has eigenvalues with negative real parts. Hence, all the poles of  $[i\omega_1 - \mathcal{L}_0]^{-1}$  in Eq. B7 are contained in the upper half plane and on the real axis. The latter poles are easily avoided if the field is time-limited.

Consider a field  $\varepsilon(t)$  compactly supported in the time-domain (time-limited), i.e.

$$\varepsilon(t) = 0 \quad \text{for } |t - t_1| > T/2 \tag{B8}$$

where  $t_1$  defines the center of an interval of size  $T$  over which the field is nonzero. Then, by the Paley-Wiener theorem,<sup>72</sup>  $\varepsilon(\omega)$  is an entire function over complex  $\omega$  and is square-integratable over horizontal lines,

$$\int_{-\infty}^{\infty} d\omega |\varepsilon(\omega - i\eta)|^2 < C. \tag{B9}$$

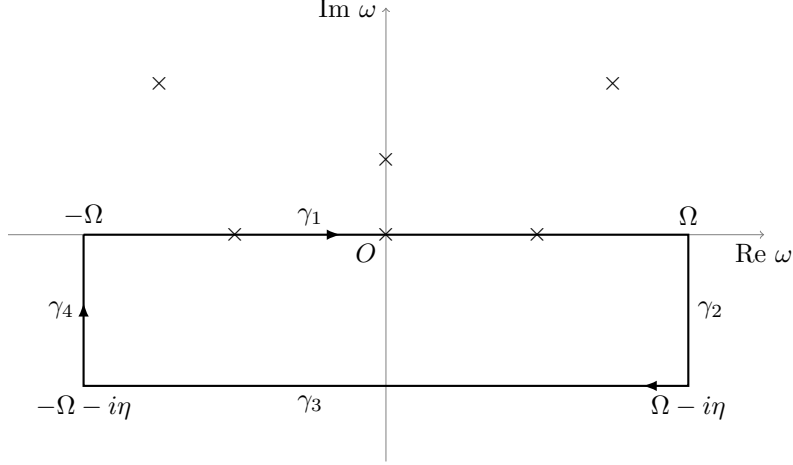


FIG. 15: Contour integral for Eq. (B5).  $\mathcal{G}_0(\omega_1)$  has poles, represented by crosses, in the upper half-plane for an open system or along the  $\text{Re } \omega_1$  axis for a closed system. The value of  $\eta > 0$  is a matter a numerical convergence.<sup>71</sup>

The integral of Eq. (B5) is given by  $\gamma_1$  in Fig. 15. By the Cauchy integral theorem,

$$\gamma_1 + \gamma_2 + \gamma_3 + \gamma_4 = 0. \quad (\text{B10})$$

As the field is square-integratable,  $\gamma_2$  and  $\gamma_4$  are zero, such that  $\gamma_1 = -\gamma_3$ . Thus, the integration of  $\omega_1$  from  $-\infty$  to  $\infty$  can instead be performed over the line from  $-\infty - i\eta$  to  $\infty - i\eta$ , where  $\eta$  is a positive real number, thereby avoiding all poles of  $\mathcal{G}_0(\omega_1)$ , provided that the field is time-limited. The following is then obtained,

$$\begin{aligned} \rho_1(t) &= \left(\frac{i}{2\pi\hbar}\right)^1 \int_{-\infty}^{\infty} d\omega_1 \varepsilon(\omega_1 - i\eta) \int_{-\infty}^{\infty} dt_1 e^{i\omega_1 t_1 + \eta t_1} \mathcal{G}_0(t - t_1) \mathcal{V} \rho_0 \\ \rho_2(t) &= \left(\frac{i}{2\pi\hbar}\right)^2 \iint_{-\infty}^{\infty} d\omega_2 d\omega_1 \varepsilon(\omega_2) \varepsilon(\omega_1 - i\eta) \iint_{-\infty}^{\infty} dt_2 dt_1 e^{i\omega_2 t_2 + i\omega_1 t_1 + \eta t_1} \mathcal{G}_0(t - t_2) \mathcal{V} \mathcal{G}_0(t_2 - t_1) \mathcal{V} \rho_0 \\ &\dots \end{aligned} \quad (\text{B11})$$

These integrals can be evaluated by applying Eq. (B5) to each time integral in sequence. The first order term (where  $t_2 = t$ ) is given by,

$$\rho_1(t) = \left(\frac{i}{2\pi\hbar}\right)^1 \int_{-\infty}^{\infty} d\omega_1 \varepsilon(\omega_1 - i\eta) e^{i\omega_1 t + \eta t} \mathcal{G}_0(\omega_1 - i\eta) \mathcal{V} \rho_0. \quad (\text{B12})$$

Some algebra yields the following higher order terms,

$$\rho_2(t) = \left(\frac{i}{2\pi\hbar}\right)^2 \iint_{-\infty}^{\infty} d\omega_2 d\omega_1 e^{i(\omega_2+\omega_1)t+\eta t} \varepsilon(\omega_2) \varepsilon(\omega_1 - i\eta) \quad (\text{B13})$$

$$\times \mathcal{G}_0(\omega_2 + \omega_1 - i\eta) \mathcal{V} \mathcal{G}_0(\omega_1 - i\eta) \mathcal{V} \rho_0$$

$$\rho_3(t) = \left(\frac{i}{2\pi\hbar}\right)^3 \iiint_{-\infty}^{\infty} d\omega_3 d\omega_2 d\omega_1 e^{i(\omega_3+\omega_2+\omega_1)t+\eta t} \varepsilon(\omega_3) \varepsilon(\omega_2) \varepsilon(\omega_1 - i\eta) \quad (\text{B14})$$

$$\times \mathcal{G}_0(\omega_3 + \omega_2 + \omega_1 - i\eta) \mathcal{V} \mathcal{G}_0(\omega_2 + \omega_1 - i\eta) \mathcal{V} \mathcal{G}_0(\omega_1 - i\eta) \mathcal{V} \rho_0$$

$$\rho_4(t) = \left(\frac{i}{2\pi\hbar}\right)^4 \iiint_{-\infty}^{\infty} d\omega_4 d\omega_3 d\omega_2 d\omega_1 e^{i(\omega_4+\omega_3+\omega_2+\omega_1)t+\eta t} \varepsilon(\omega_4) \varepsilon(\omega_3) \varepsilon(\omega_2) \varepsilon(\omega_1 - i\eta) \quad (\text{B15})$$

$$\times \mathcal{G}_0(\omega_4 + \omega_3 + \omega_2 + \omega_1 - i\eta) \mathcal{V} \mathcal{G}_0(\omega_3 + \omega_2 + \omega_1 - i\eta)$$

$$\times \mathcal{V} \mathcal{G}_0(\omega_2 + \omega_1 - i\eta) \mathcal{V} \mathcal{G}_0(\omega_1 - i\eta) \mathcal{V} \rho_0$$

...

Every term of the perturbative expansion converges when the field is time-limited, as is the case here.

The effect that the system has on the outgoing electric field is computed below using the microscopic equations, under the assumption that the sample is highly dilute.<sup>42</sup> Consider the change in the energy of the controlled system due to radiation,

$$\Delta E_s(t) = -\frac{d\varepsilon(t)}{dt} \text{Tr} \mu \rho(t) \quad (\text{B16})$$

Using the Fourier representation of the field, the following is obtained,

$$\Delta E_s(t) = \frac{1}{2\pi i} \int_{-\infty}^{\infty} d\omega (-\omega) \varepsilon^*(\omega) \text{Tr} \mu \rho(t) e^{-i\omega t} \quad (\text{B17})$$

A gain of energy by the system must be balanced by a corresponding loss in the electric field. The overall change in the energy of radiation after interacting with the system is then given by,

$$\Delta E_r = - \int_{-\infty}^{\infty} dt \Delta E_s(t) \quad (\text{B18})$$

The  $n$ -th order contribution in the electric field can then be obtained from the  $n-1$  density matrix,

$$\Delta E_r^{(n)} = \frac{1}{2\pi i} \int_{-\infty}^{\infty} d\omega \omega \varepsilon^*(\omega) \text{Tr} \mu \rho^{(n-1)}(\omega) \quad (\text{B19})$$

The change in the overall energy of the field after encountering a single molecule is expressed as a change in the number of photons in mode  $\omega$  times the energy of photons in that mode,

$$\Delta E_r^{(n)} = \int_{-\infty}^{\infty} d\omega N_{\Delta}^{(n)}(\omega) \hbar \omega \quad (\text{B20})$$

with the following spectrally-resolved change in the photon flux due to interactions of order  $n$ ,

$$N_{\Delta}^{(n)}(\omega) = \frac{1}{2\pi\hbar i} \varepsilon^*(\omega) \text{Tr} \mu \rho^{(n-1)}(\omega). \quad (\text{B21})$$

The change in the spectral photon flux  $N_{\Delta}(\omega)$  is the sum of the second and fourth order contributions  $N_{\Delta}^{(2)}(\omega) + N_{\Delta}^{(4)}(\omega)$ .

The weak-field perturbative expansion [Eqs. (B12) to (B15)] has a few important features, which warrants its use for numerical work as well as for analytical calculations, even though it is more complicated than a direct numerical computation. Indeed, perturbation theory can be avoided numerically by simply evolving the semiclassical Liouvillian given by Eq. (6) directly. However, the direct method is problematic for three reasons: (a) at higher excitation intensities, the density matrix may contain undesired higher order contributions; (b) at lower excitation intensities numerical errors can drastically affect the very small excited state populations, requiring fine numerical tolerances, and (c) measuring the scaling of control with intensity requires repeated computations, which can rapidly (due to the previous two issues) become computationally expensive and numerically difficult. These issues are avoided by a numerical computation of the perturbative series. Furthermore, the absorption spectrum and other nonlinear spectroscopic properties are more easily calculated perturbatively, especially when multiple spatial or polarization components of the field are included.<sup>42</sup>

The numerical evaluation of Eqs. (B12) to (B15) is difficult due to the high-dimensionality of the frequency integrations. As seen above, the perturbative expansion of  $\rho(t)$  for weak-field two-photon processes requires the evaluation of a four-dimensional frequency integrals. Additionally, the Green's function above may have poles on the real frequency axis, further frustrating numerical efforts. For these reasons, we have developed the algorithm described in Ref. 71, which avoids all of these issues. This numerical method was successfully used to obtain the results described in this paper.

## Appendix C: Minimal models for two-photon phase control

Three control models are used in Sec. III A. The models consists of five levels (Fig. 4a). Dissipation and decoherence are included to obtain sub-unity quantum yields and continuous lineshapes. The following Lindblad relaxation tensor is defined,

$$\mathcal{R}_L \rho = \sum_k \gamma_k \left( L_k \rho L_k^\dagger - \frac{1}{2} \left\{ L_k^\dagger L_k, \rho \right\} \right) \quad (\text{C1})$$

The material Liouvillian of Eq. (6) is then given by

$$\mathcal{L}_0 \rho = \frac{1}{i\hbar} [H_0, \rho] + \mathcal{R}_L \rho. \quad (\text{C2})$$

The decoherence terms are given by,

$$L_k = |k\rangle \langle k| \quad (\text{C3})$$

where  $k$  runs over all indices of the field and the corresponding rate is given by  $\gamma_k = 2/\tau_{\text{deco}}$ . The electronic excited state has a short electronic decoherence time  $\tau_{\text{el,deco}}$  while the remaining states are assigned a slower vibrational decoherence time  $\tau_{\text{vib,deco}}$ . The dissipation operator for the  $i \rightarrow j$  relaxation has the form,

$$L_{i \rightarrow j} = |j\rangle \langle i|. \quad (\text{C4})$$

The dissipation rate for the  $|v\rangle$  to  $|g\rangle$  relaxation is  $\gamma_{\text{diss}} = 1/\tau_{\text{diss}}$ . The excited state  $|e\rangle$  relaxes to  $|t\rangle$  with a rate of  $\text{QY}_e \gamma_{\text{diss}}$  and to  $|g\rangle$  with a rate of  $(1 - \text{QY}_e) \gamma_{\text{diss}}$ . Similarly, the relaxation rate from  $|t\rangle$  to  $|p\rangle$  is given by  $\text{QY}_t \gamma_{\text{diss}}$  and from  $|t\rangle$  to  $|g\rangle$  by  $(1 - \text{QY}_t) \gamma_{\text{diss}}$ . These parameters are also described in Table II.

The light-matter coupling superoperator is given by

$$\varepsilon(t) \mathcal{V} \rho = \varepsilon(t) [\mu, \rho] = E_0 \mu_0 E(t) [u, \rho] \quad (\text{C5})$$

where  $u = \mu/\mu_0$  and  $E(t) = \varepsilon(t)/E_0$  are dimensionless. The parameter  $E_0 \mu_0$  tracks the perturbation strength and has units of energy. Matrix elements of  $u$  are given in Table II. The field function  $E(t)$  is given in the frequency domain by

$$E(\omega) = g(\omega; \omega_0, \sigma, \chi) + g(\omega; -\omega_0, \sigma, -\chi) \quad (\text{C6})$$

	$E_v$	$E_t$	$u_{gv}$	$u_{ve}$	$u_{et}$	$u_{gt}$	$u_{tp}$
2 vs. 2	1.36	1.40	0.01	1.00	—	—	—
1 vs. 3	0.8	1.35	0.01	1.00	1.00	0.0002	—
Pump-dump	0.8	1.40	—	—	—	0.01	1.00
	$E_g$	$E_e$	$E_p$	$u_{ge}$			
All control scenarios	0.0	2.76	0.10	—			
	$\tau_{\text{el,deco}}$	$\tau_{\text{vib,deco}}$	$\tau_{\text{diss}}$	$\text{QY}_e$	$\text{QY}_t$		
	90 fs	500 fs	1000 fs	0.5	0.8		

TABLE II: Parameters for each of the three control scenarios corresponding to the three mechanisms described in the text. Energies are in  $eV$  while quantum yields  $\text{QY}_t$  and  $\text{QY}_e$  and transition strengths  $u_{ij}$  are dimensionless.

	$\mu_0 E_0$	$\hbar\omega_0$	$\text{FWHM}_t$
Control scenarios <sup>†</sup>	0.05 eV	1.38 eV	80 fs
Retinal/ChR2 model*	0.047 eV	1.25 eV	120 fs

<sup>†</sup>:  $\mu_0 E_0$  is 0.20 eV for the pump-dump case.

\* : Visible absorption (Fig. 11a) computed using  $\hbar\omega_0 = 2.5$  eV.

TABLE III: Parameters of the fields used throughout.

where the function  $g(\omega; \omega_0, \sigma, \chi)$  is a dimensionless, normalized Gaussian with chirp  $\chi$ :

$$g(\omega; \omega_0, \sigma, \chi) = \frac{1}{(2\sigma)^{1/2}\pi^{1/4}} \exp\left(-\frac{(\omega - \omega_0)^2}{2\sigma^2} - i\chi(\omega - \omega_0)^2\right) \quad (\text{C7})$$

The standard deviation of the field  $\sigma$  in the Fourier domain is computed from the FWHM in the time domain as,

$$\sigma = \frac{2\sqrt{2\log 2}}{\text{FWHM}_t} \quad (\text{C8})$$

Parameters of the field are given in Table III.

## Appendix D: Two-photon control of retinal isomerization

The two-photon photoisomerization of retinal is computed from the one vibrational mode and two electronic state model of Ref. 34. The molecular Hamiltonian is given by

$$H_0(\phi) = -\frac{1}{2I} \begin{pmatrix} \frac{\partial^2}{\partial \phi^2} & 0 \\ 0 & \frac{\partial^2}{\partial \phi^2} \end{pmatrix} + \begin{pmatrix} \alpha_1(1 - \cos \phi) & \lambda \\ \lambda & E_2 - \alpha_2(1 - \cos \phi) \end{pmatrix} \quad (\text{D1})$$

where  $\phi$  is a torsional mode with angles from 0 to  $2\pi$ . The *trans* and *cis* subspaces are defined by the following projectors,

$$P_{\text{trans}}(\phi) = \begin{cases} 1 & \text{for } |\phi| < \pi/2 \\ 0 & \text{otherwise} \end{cases} \quad (\text{D2})$$

$$P_{\text{cis}}(\phi) = 1 - P_{\text{trans}}(\phi) \quad (\text{D3})$$

It should be noted that this is the opposite of the definitions of Ref. 34 since the ground state of retinal in channelrhodopsin is the *trans* state.<sup>8</sup> To keep the number of adjustable parameters to a minimum, only the *cis* and *trans* labels from Ref. 34 were changed. Two-photon absorption, c.f. eqs. (27)-(29), is obtained by adding a near-resonant state at energy  $E_v$ . Light-matter coupling is computed with eqs. (C5)-(C8) above. The transition operator in this case is given by

$$u = a_e |g\rangle \langle e| + a_v |g\rangle \langle v| + \text{h.c.} \quad (\text{D4})$$

Eq. (29) is satisfied by setting  $\mu_0 E_0 = 0.047$  eV and the ratio  $|a_v|^2/|a_e|^2$  to 1/86. Model parameters are given Table IV and field parameters in Table III.

The retinal environment that stabilizes the *cis* and *trans* isomers is evaluated in the secular Redfield approximation<sup>46</sup> and integrated as part of the Green's function calculation in the same manner as the Lindblad tensors above. The system part of the system-bath coupling is given by the following dimensionless operator,

$$V_{sb} = \begin{pmatrix} \sqrt{1-y}(\cos \phi) & 0 \\ 0 & \sqrt{y}(1 - \cos \phi) \end{pmatrix} \quad (\text{D5})$$

where the  $\cos \phi$  part selects for the *trans* configuration,  $1 - \cos \phi$  for the *cis* configuration and  $y$  is a dimensionless parameter that determines the yield of the photoisomerization. The

Retinal	$I$	$\alpha_1$	$\alpha_2$	$E_2$	$\lambda$	$E_v^\dagger$
	$4.84 \times 10^{-4}$	3.6	1.09	2.48	0.065	1.22
Environment	$\eta$	$\omega_c$	$y^\dagger$			
	0.45	0.035	0.8			

†: Parameter modified from or not found in Ref. 34.

TABLE IV: Parameters of the microscopic model of retinal<sup>34</sup> used to compute two-photon activation rates. The yield parameter  $y$  is dimensionless; every other value is in eV.

bath spectral density is ohmic with a cutoff, given by

$$J(\omega) = \eta \omega e^{-\omega/\omega_c}. \quad (\text{D6})$$

The temperature of the Bose-Einstein bath is set to absolute zero. This ensures that both the cis and trans states are steady states. Indeed, this standard model does not otherwise reproduce the extremely long-lived trans quasi-steady state of retinal in channelrhodopsins,<sup>7</sup> which is critical to the repeated interaction amplification of control, as described in eq. (4).

## REFERENCES

- <sup>1</sup>M. Shapiro and P. Brumer, *Quantum Control of Molecular Processes* (John Wiley & Sons, 2012).
- <sup>2</sup>L. Zhu, V. Kleiman, X. Li, S. P. Lu, K. Trentelman, and R. J. Gordon, *Science* **270**, 77 (1995).
- <sup>3</sup>A. Haché, Y. Kostoulas, R. Atanasov, J. L. P. Hughes, J. E. Sipe, and H. M. van Driel, *Phys. Rev. Lett.* **78**, 306 (1997).
- <sup>4</sup>T. H. Stievater, X. Li, D. G. Steel, D. Gammon, D. S. Katzer, D. Park, C. Piermarocchi, and L. J. Sham, *Phys. Rev. Lett.* **87**, 133603 (2001).
- <sup>5</sup>D. Brinks, F. D. Stefani, F. Kulzer, R. Hildner, T. H. Taminiau, Y. Avlasevich, K. Müllen, and N. F. van Hulst, *Nature* **465**, 905 (2010).
- <sup>6</sup>K. Paul, P. Sengupta, E. D. Ark, H. Tu, Y. Zhao, and S. A. Boppart, *Nat. Phys.* **13**, 1111 (2017).
- <sup>7</sup>V. A. Lórenz-Fonfría and J. Heberle, *BBA - Bioenergetics* **1837**, 626 (2014).
- <sup>8</sup>F. Schneider, C. Grimm, and P. Hegemann, *Annu. Rev. Biophys.* **44**, 167 (2015).

- <sup>9</sup>C. A. Arango and P. Brumer, *J. Chem. Phys.* **138**, 071104 (2013).
- <sup>10</sup>J. L. Herek, W. Wohlleben, R. J. Cogdell, D. Zeidler, and M. Motzkus, *Nature* **417**, 533 (2002).
- <sup>11</sup>V. I. Prokhorenko, A. M. Nagy, S. A. Waschuk, L. S. Brown, R. R. Birge, and R. J. D. Miller, *Science* **313**, 1257 (2006).
- <sup>12</sup>P. J. M. Johnson, A. Halpin, T. Morizumi, V. I. Prokhorenko, O. P. Ernst, and R. J. D. Miller, *Nat. Chem.* **7**, 980 (2015).
- <sup>13</sup>M. Izquierdo-Serra, M. Gascón-Moya, J. J. Hirtz, S. Pittolo, K. E. Poskanzer, È. Ferrer, R. Alibés, F. Busqué, R. Yuste, J. Hernando, and P. Gorostiza, *J. Am. Chem. Soc.* **136**, 8693 (2014).
- <sup>14</sup>E. C. Carroll, S. Berlin, J. Levitz, M. A. Kienzler, Z. Yuan, D. Madsen, D. S. Larsen, and E. Y. Isacoff, *PNAS* **112**, E776 (2015).
- <sup>15</sup>Z. Wei, L. He, Z. Chi, X. Ran, and L. Guo, *Spectrochim. Acta A* **206**, 120 (2019).
- <sup>16</sup>J. C. Scaiano, L. J. Johnston, W. G. McGimpsey, and D. Weir, *Acc. Chem. Res.* **21**, 22 (1988).
- <sup>17</sup>I. Pastirk, E. J. Brown, Q. Zhang, and M. Dantus, *J. Chem. Phys.* **108**, 4375 (1998).
- <sup>18</sup>V. K. Potapov and V. M. Matyuk, *High Energ. Chem.* **35**, 90 (2001).
- <sup>19</sup>I. Pastirk, J. M. D. Cruz, K. A. Walowicz, V. V. Lozovoy, and M. Dantus, *Opt. Express* **11**, 1695 (2003).
- <sup>20</sup>L. T. Schelhas, J. C. Shane, and M. Dantus, *Nanomed. Nanotechnol.* **2**, 177 (2006).
- <sup>21</sup>J. P. Ogilvie, D. Débarre, X. Solinas, J.-L. Martin, E. Beaurepaire, and M. Joffre, *Opt. Express* **14**, 759 (2006).
- <sup>22</sup>E. R. Tkaczyk, A. H. Tkaczyk, K. Mauring, J. Y. Ye, J. R. Baker, and T. B. Norris, *J. Fluoresc.* **19**, 517 (2009).
- <sup>23</sup>K. Isobe, A. Suda, M. Tanaka, F. Kannari, H. Kawano, H. Mizuno, A. Miyawaki, and K. Midorikawa, *Opt. Express* **17**, 13737 (2009).
- <sup>24</sup>M. H. Brenner, D. Cai, J. A. Swanson, and J. P. Ogilvie, *Opt. Express* **21**, 17256 (2013).
- <sup>25</sup>O. Katz, E. Small, Y. Bromberg, and Y. Silberberg, *Nat. Photon.* **5**, 372 (2011).
- <sup>26</sup>M. Mounaix, D. Andreoli, H. Defienne, G. Volpe, O. Katz, S. Grésillon, and S. Gigan, *Phys. Rev. Lett.* **116**, 253901 (2016).
- <sup>27</sup>M. Shapiro and P. Brumer, *J. Chem. Phys.* **103**, 487 (1995).
- <sup>28</sup>M. Spanner, C. A. Arango, and P. Brumer, *J. Chem. Phys.* **133**, 151101 (2010).

- <sup>29</sup>K. Hoki and P. Brumer, Phys. Rev. Lett. **95**, 168305 (2005).
- <sup>30</sup>C. Lavigne and P. Brumer, J. Chem. Phys. **147**, 114107 (2017).
- <sup>31</sup>The case of two-photon coherent control using continuous-wave lasers is described in e.g., Z. Chen, P. Brumer, and M. Shapiro, Chem. Phys. Lett. **198**, 498 (1992); Z. Chen, M. Shapiro, and P. Brumer, J. Chem. Phys. **98**, 8647 (1993); Z. Chen, P. Brumer, and M. Shapiro, J. Chem. Phys. **98**, 6843 (1993).
- <sup>32</sup>S. Hahn and G. Stock, J. Phys. Chem. B **104**, 1146 (2000).
- <sup>33</sup>S. Hahn and G. Stock, J. Chem. Phys **116**, 1085 (2002).
- <sup>34</sup>B. Balzer, S. Hahn, and G. Stock, Chem. Phys. Lett. **379**, 351 (2003).
- <sup>35</sup>K. Nikolic, N. Grossman, M. S. Grubb, J. Burrone, C. Toumazou, and P. Degenaar, Photochem. Photobiol. **85**, 400 (2009).
- <sup>36</sup>B. D. Evans, S. Jarvis, S. R. Schultz, and K. Nikolic, Front. Neuroinform. **10** (2016), 10.3389/fninf.2016.00008.
- <sup>37</sup>N. Grossman, K. Nikolic, C. Toumazou, and P. Degenaar, IEEE T. Biomed. Eng. **58**, 1742 (2011).
- <sup>38</sup>T. J. Foutz, R. L. Arlow, and C. C. McIntyre, J. Neurophysiol. **107**, 3235 (2012).
- <sup>39</sup>J. P. Rickgauer and D. W. Tank, PNAS **106**, 15025 (2009).
- <sup>40</sup>M.-K. Verhoeven, C. Bamann, R. Blöcher, U. Förster, E. Bamberg, and J. Wachtveitl, ChemPhysChem **11**, 3113 (2010).
- <sup>41</sup>M.-K. Neumann-Verhoeven, K. Neumann, C. Bamann, I. Radu, J. Heberle, E. Bamberg, and J. Wachtveitl, J. Am. Chem. Soc. **135**, 6968 (2013).
- <sup>42</sup>S. Mukamel, *Principles of Nonlinear Optical Spectroscopy* (Oxford University Press, 1995).
- <sup>43</sup>C. Xu and W. W. Webb, J. Opt. Soc. Am. B **13**, 481 (1996).
- <sup>44</sup>The mechanism of ChR2 activation is quite complex.<sup>8</sup> For simplicity, we assume here that the photoisomerization of a retinal in a closed-state ChR2 always produce the open state.
- <sup>45</sup>C. Bamann, T. Kirsch, G. Nagel, and E. Bamberg, J. Mol. Biol. **375**, 686 (2008).
- <sup>46</sup>U. Weiss, *Quantum Dissipative Systems* (World Scientific, 2012).
- <sup>47</sup>D. Meshulach and Y. Silberberg, Nature **396**, 239 (1998).
- <sup>48</sup>V. V. Lozovoy, I. Pastirk, K. A. Walowicz, and M. Dantus, J. Chem. Phys **118**, 3187 (2003).
- <sup>49</sup>There is no accepted definition for the quantum yield in a pump-dump experiment. The quantum yield of the pump-dump control scheme is here above unity as less than one

- photon is used per product obtained; a significant portion of absorbed “pump” photons are re-emitted by stimulated emission.
- <sup>50</sup>The one-photon absorption to  $|t\rangle$  is 2500 times weaker than resonant absorption to  $|v\rangle$ .
- <sup>51</sup>R. R. Birge and T. M. Cooper, *Biophys. J.* **42**, 61 (1983).
- <sup>52</sup>R. R. Birge, T. M. Cooper, A. F. Lawrence, M. B. Masthay, C. F. Zhang, and R. Zidovetzki, *J. Am. Chem. Soc.* **113**, 4327 (1991).
- <sup>53</sup>R. R. Birge and C.-F. Zhang, *J. Chem. Phys.* **92**, 7178 (1990).
- <sup>54</sup>G. Palczewska, F. Vinberg, P. Stremplewski, M. P. Bircher, D. Salom, K. Komar, J. Zhang, M. Cascella, M. Wojtkowski, V. J. Kefalov, and K. Palczewski, *PNAS* **111**, E5445 (2014).
- <sup>55</sup>G. Nagel, T. Szellas, W. Huhn, S. Kateriya, N. Adeishvili, P. Berthold, D. Ollig, P. Hegemann, and E. Bamberg, *PNAS* **100**, 13940 (2003).
- <sup>56</sup>The  $|g\rangle \rightarrow |v\rangle$  transition must be resonant to obtain chirp control. Whether its frequency is above or below the central frequency of the laser determines whether absorption is maximal at negative or positive chirps. The latter is chosen here to match the result of Ref. 6.
- <sup>57</sup>One-photon excitations to  $|v\rangle$  relax non-productively to  $|g\rangle$  so that modifying  $a_v$  does not change the one-photon contribution to isomerization. In addition, as there are no other near-resonant transitions in the model, two-photon absorption primarily occurs through  $|v\rangle$ , such that the two-photon absorption probability is proportional to  $|a_v|^2$ .
- <sup>58</sup>P. Brumer and M. Shapiro, *Chem. Phys.* **139**, 221 (1989).
- <sup>59</sup>M. Liebel and P. Kukura, *Nat. Chem.* **9**, 45 (2017).
- <sup>60</sup>C. Lavigne and P. Brumer, *In prep.* (2019).
- <sup>61</sup>O. Vendrell and H.-D. Meyer, *J. Chem. Phys.* **134**, 044135 (2011).
- <sup>62</sup>P. S. Christopher, M. Shapiro, and P. Brumer, *J. Chem. Phys.* **124**, 184107 (2006).
- <sup>63</sup>C. Lavigne, *QP Partitioning for Radiationless Transitions*, Msc Thesis, University of Toronto (2014).
- <sup>64</sup>J. Shao and N. Makri, *J. Chem. Phys.* **116**, 507 (2002).
- <sup>65</sup>L. A. Pachón and P. Brumer, *J. Chem. Phys.* **139**, 164123 (2013).
- <sup>66</sup>J. Ma and J. Cao, *J. Chem. Phys.* **142**, 094106 (2015).
- <sup>67</sup>J. Ma, J. Moix, and J. Cao, *J. Chem. Phys.* **142**, 094107 (2015).
- <sup>68</sup>J. M. Moix, J. Ma, and J. Cao, *J. Chem. Phys.* **142**, 094108 (2015).
- <sup>69</sup>E. Papagiakoumou, F. Anselmi, A. Bègue, V. de Sars, J. Glückstad, E. Y. Isacoff, and V. Emiliani, *Nat. Methods* **7**, 848 (2010).

- <sup>70</sup>S. Sakadžić, E. Roussakis, M. A. Yaseen, E. T. Mandeville, V. J. Srinivasan, K. Arai, S. Ruvinskaya, A. Devor, E. H. Lo, S. A. Vinogradov, and D. A. Boas, *Nat. Methods* **7**, 755 (2010).
- <sup>71</sup>C. Lavigne and P. Brumer, arXiv:1907.07734 [physics] (2019), arXiv:1907.07734 [physics].
- <sup>72</sup>W. Rudin, *Real and Complex Analysis* (McGraw-Hill, 1987).